THESIS APPROVAL

The abstract and thesis of Jake Griffiths for the Master of Science in Geology presented August 9, 2002, and accepted by the thesis committee and the department.

COMMITTEE APPROVALS:

Kenneth M. Cruikshank, Chair

Michael L. Cummings

Christina L. Hulbe

Michael E. Emch
Representative of the Office of Graduate Studies

DEPARTMENTAL APPROVAL:

Michael L. Cummings
Department of Geology

Abstract

An abstract of the thesis of Jake Griffiths for the Master of Science in Geology presented August 9, 2002

Title: ANALYSIS OF A KINK-LIKE FOLD IN THE OREGON-IDAHO GRABEN, MALHEUR COUNTY, OREGON

The Oregon-Idaho graben is a north-striking structural depression extending from eastern Oregon into western Idaho. During it's evolution the graben developed a series of sub-basins, separated by north-striking intragraben fault zones. On average, intragraben fault zones have throws greater than 1 km, but are composed of individual faults with throws ranging from 1 to 10 m. Many of the faults are vertical; therefore, throw on these faults produces little shortening or extension normal to their strike. NE-striking kink-like folds are present within these fault zones. One of these faulted-kinks, here informally called the *trap-door structure*, is within the Dry Creek Buttes intragraben fault zone along the north shore of the Dry Creek arm of Lake Owyhee and is the topic of this thesis.

The trap-door structure was mapped at 1:3650 and a series of down-plunge views were constructed along strike. At its southern margin, the trap-door structure has dip changes greater than 35° from the regional dip; mafic sills and dikes on the western limb; sharply kinked layers in the middle; and relatively constant dip on the eastern limb, a geometry similar to Laramide folds on the Colorado Plateau. This geometry is similar along strike to the north.

The geometry of the trap-door structure is consistent with the geometry expected for deformation above the margins of sill-like intrusions or above two buried faults. However, recognizing consistent NE orientation of kink-like folds throughout the Oregon-Idaho graben, the high-angle faults, and structural evolution of the Dry Creek Buttes fault zone, displacement on buried faults is the most likely explanation for the trap-door structure. Numerical modeling and the mapped geometry indicate that a pair of NE-striking *en echelon* faults is buried beneath the trap-door structure. The fault-blocks are 0.24 km to 0.77 km deep, and have displacements ranging from 0.225 km to 0.320 km.

ANALYSIS OF A KINK-LIKE FOLD IN THE OREGON-IDAHO GRABEN, MALHEUR COUNTY, OREGON

by

JAKE GRIFFITHS

A thesis submitted in partial fulfillment of the
requirements for the degree of

MASTER OF SCIENCE
in
GEOLOGY

Portland State University
2002

Dedication

This thesis is dedicated to my family

Linda V. Cornelius, my mother, who never doubted my interests;

Cary L. Griffiths, my father, who taught me to be persistent;

Darin L. Griffiths, my brother, whom I cherish for his strength; and

Rachael A. Griffiths, my sister, for her curious mind.

Acknowledgments

The Paul Howell Award from the Department of Geology at Portland State University, and Kenneth M. Cruikshank supported this work. Ken's enduring mentorship above all things taught me how to use the scientific method. His good judgment, patience, optimism, and enthusiasm for science are all invigorating. Thank you Ken! In addition to formal assistance by being a part of the committee, Michael L. Cummings proffered unyielding interest and assistance in early versions of this thesis. Christina L. Hulbe has wonderful insight and adds excitement to using models. Thanks to Kimberly Paige Shell-Spurling and Patricia Ann Zensen for help in the field. Thanks to Arvid M. Johnson for making available the Purdue Faux-Pli folding suite. Accordingly, thanks to Kaj M. Johnson for help with the model.

Table of Contents

List of Figures

List of Tables

1. Introduction

The Oregon-Idaho graben is situated along the Oregon-Idaho border in the western United States (Figure 1). It is a 50 km-wide, 100 km-long structural depression that developed concurrently with the eruption of volcanic rocks during the Miocene (Cummings et al., 2000). The structural evolution includes the growth of three north-striking intragraben fault zones, which are, from west to east: Wall Rock Ridge, Dry Creek Buttes, and Devils Gate (Cummings et al., 2000). Squaw Creek fault zone is the western proximity of the Oregon-Idaho graben (Cummings et al., 2000). The intragraben fault zones are nearly vertical. This suggests that the fault zones were not important factors in extension normal to the axis of the graben. On average, the fault-zones have throws greater than 1 km, but are composed of individual faults that have throws ranging from 1 to 10 m (Cummings et al., 2000). Lake Owyhee is located in the Dry Creek Buttes fault zone (Figure 1). Additionally, my field mapping, north of Nanny's Nipple and west of Burnt Mountain (Figure 2), has revealed a NE-striking faulted kink-like fold (here informally called the *trap-door structure*). It is located along the north shore of the Dry Creek Arm of Lake Owyhee, Malheur County, Oregon (Figure 2). Hess (1998) observed other faulted kink-like folds at Burnt Mountain and to the south of Lake Owyhee. The structures described here are part of the Dry Creek Buttes fault zone (Cummings et al., 2000).

The first part of this thesis presents the results of 1:3650 mapping of the trap-door structure. The second part presents the results from numerical modeling that suggests how this structure, and others in the area, could have formed.

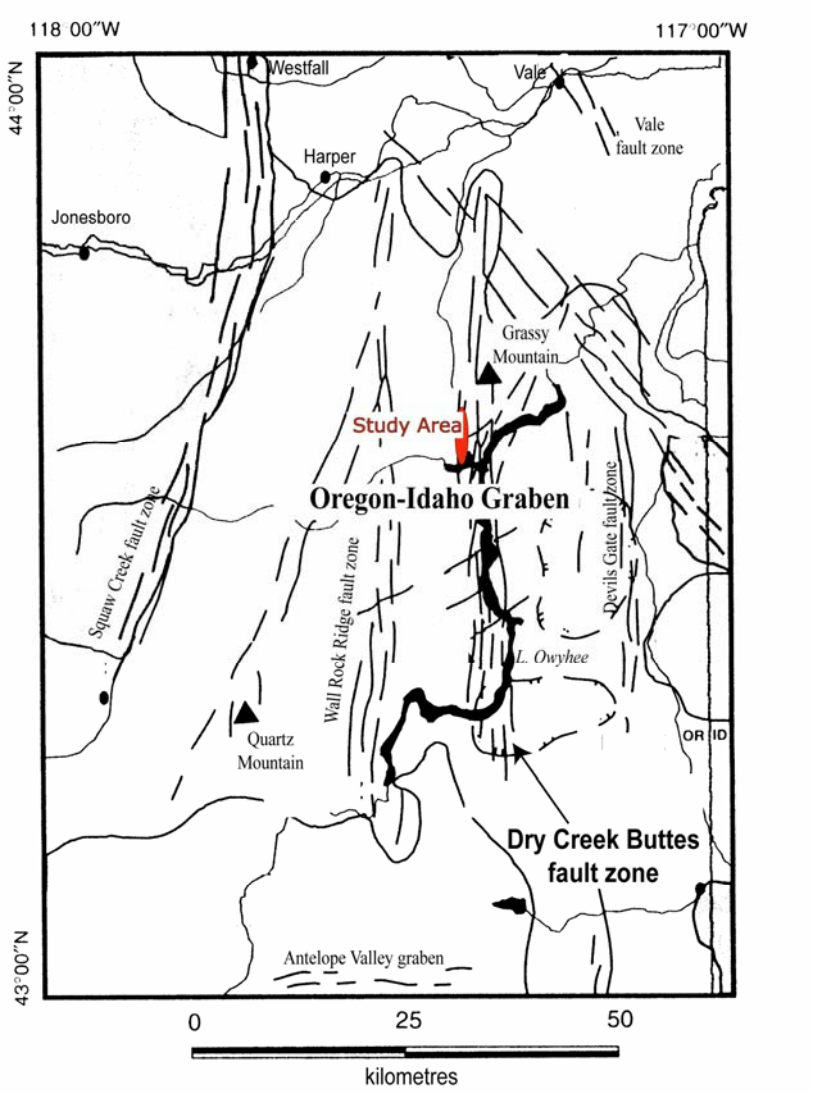

Figure 1. General fault map of the Oregon-Idaho graben. My study area is approximately 3 km southwest of Grassy Mountain (Cummings et al., 2000).

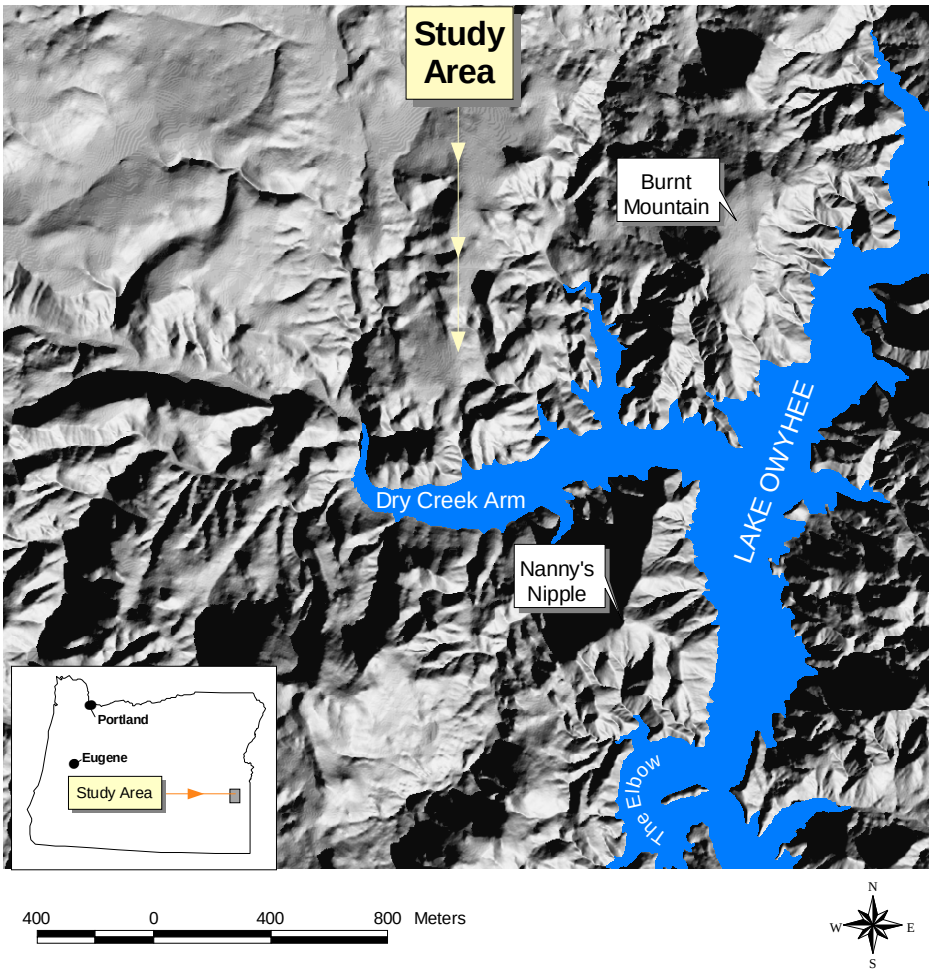

Figure 2. The trap-door structure is located north of Dry Creek Arm of Lake Owyhee, approximately 1 km west of Burnt Mountain and 1.5 km north of Nanny's Nipple. NNW-striking lineaments on the image are west-facing scarps, which are topographic expressions of some of the faults in this area.

2. Graben Development

The Oregon-Idaho graben is located within the Owyhee Uplands (Figure 3) physiographic province (Orr and Orr, 1999). Surrounding provinces are the Basin and Range to the southwest, the High Lava Plains to the west, and the Blue Mountains to the north. The western Snake River plain lies to the northeast, in Oregon and Idaho; the Owyhee Mountains are to the east, in Idaho.

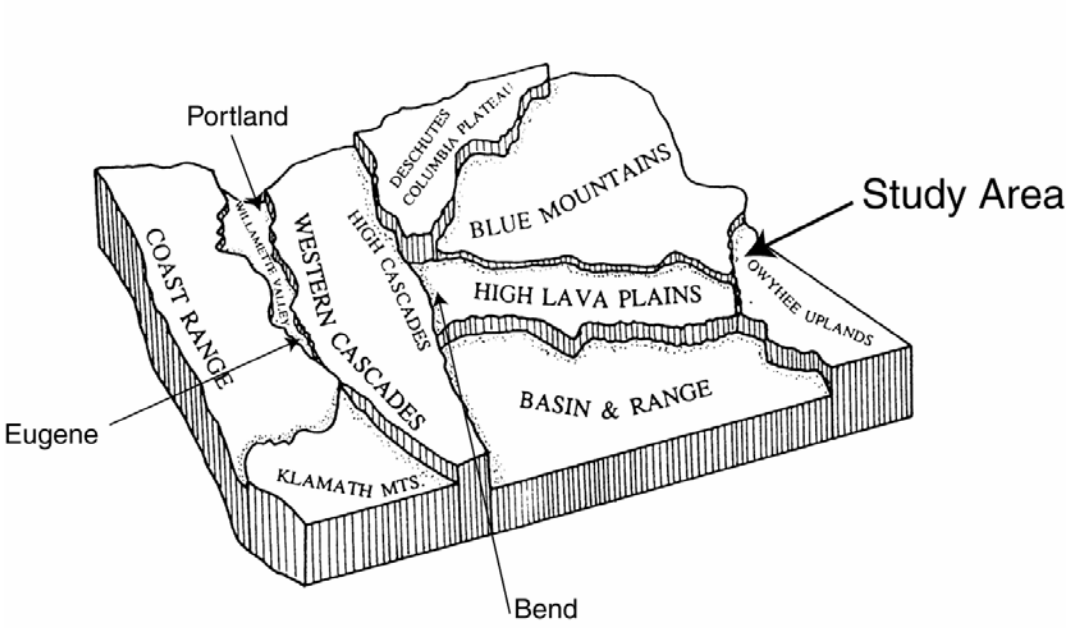

Figure 3. Physiographic provinces of Oregon (Orr and Orr, 1999).

The Oregon-Idaho graben evolved as part of a middle Miocene synvolcanic rift in a region of bimodal volcanism (Cummings et al., 2000). Subsidence began shortly after the eruption of the Grande Ronde Formation of the Columbia River Basalt Group (Cummings et al., 2000). Following initial subsidence, calc-alkaline volcanic rocks were erupted. Also, approximately 150 km west of the Oregon-Idaho graben, in Malheur River gorge, the Steens basalt and basalt of Malheur Gorge flowed over early

Miocene calc-alkaline volcanic rocks (Evans, 1990a; Evans, 1990b; Lees, 1990). The lower rocks of the basalt of Malheur Gorge are equivalent in chemistry and age to some of the Imnaha flows of the Columbia River Basalt Group (Evans, 1990a; Evans, 1990b; Lees, 1990).

Tectonism outside the Oregon-Idaho graben included uplift and volcanism in central Oregon and western Idaho, respectively (Ekren et al., 1982; Walker and Robinson, 1990; Cummings et al., 2000). The Blue Mountains region of central Oregon experienced NW-SE shortening, while rhyolitic rocks were erupted in western Idaho (Walker and Robinson, 1990; Camp et al., 2000; Cummings et al., 2000).

2.1 Structural and Stratigraphic Evolution

The stratigraphy in the Oregon-Idaho graben indicates the graben developed in three stages, and was most structurally and volcanically dynamic during the second stage (Cummings et al., 2000). During the second stage locally erupted basalt flows, hydrovolcanic complexes, and intervening lacustrine and fluvial deposits dominated the intragraben fault zones. As the second stage progressed, three intragraben fault zones—Wall Rock Ridge, Dry Creek Buttes, and the Devils Gate fault zones—became dominant (Figure 1) (Hess, 1998; Cummings et al., 2000). The fault zones exerted significant influence on volcanism and sedimentation by segmenting the graben into a series of sub-basins, while also influencing the locus of hydrothermal activity. The evolution of the Oregon-Idaho graben, summarized from (Cummings et al., 2000) is recorded below.

2.1.1 Stage One

According to Cummings et al. (2000), stage one was dominated by structural subsidence and deposition of muscovite-bearing sandstone, siltstone, and mudstone following formation of the Mahogany Mountain and Three Fingers calderas. The presence of muscovite in this unit marks the first invasion of sediment from sources located in the Owyhee Mountains of southwestern Idaho. Moreover, small-volume basalt hydrovolcanic deposits were produced by eruptions within developing intragraben fault zones, while weak angular unconformities suggest syndepositional deformation along these fault zones.

2.1.2 Stage Two

Marked by increased basalt hydrovolcanism and the abrupt disappearance of muscovite-bearing sedimentary rocks, stage two was tectonically and volcanically the most dynamic period in the graben development. In this stage, the Oregon-Idaho graben was broken into 15-20 km-wide horsts-and-grabens, each with independent histories of volcanism and sedimentation. Renewed subsidence corresponds with syntectonic calc-alkalic volcanism, the first eruption having been the Owyhee Basalt, the most voluminous unit. The Owyhee Basalt (14-15.4 Ma)—basalt and basaltic andesite—crops out immediately east of the study area. By 12.6 Ma subsidence associated with stage two had waned; stratigraphy suggests that displacement along the Dry Creek Buttes fault zone was down to the east prior to the eruption of the

Owyhee Basalt, then down to the west after the eruption of the Owyhee Basalt (Cummings et al., 2000).

Basalt hydrovolcanism centered on evolving 2-3 km wide intragraben fault zones produced tuff cones whose intermediate and distal facies interfingers with fluvial and lacustrine sediments in local basins. From these stratigraphic relations, Cummings (1991a) identified two intragraben fault zones: Wall Rock Ridge and Dry Creek Buttes.

The Wall Rock Ridge, Dry Creek Buttes, and the Devils Gate fault zones are the most prominent intragraben fault zones (Cummings et al., 2000). They are north striking and each typically consists of 2-3 km-wide zones of closely spaced steeply dipping faults (Cummings et al., 2000). The fault zones may have been initially composed of few faults, each having less than 10 m of throw.

Kink-like structures evolved along the Wall Rock Ridge and Dry Creek Buttes fault zones. The trap-door structure and a set of prominent kink-like folds described by Hess (1998)—1.5 km east of the trap-door structure—are present within the Dry Creek Buttes fault zone.

2.1.3 Stage Three

In this stage, local basins accommodated renewed lacustrine and fluvial systems. Again, muscovite-bearing siltstone and sandstone suggests invasion of sediments from the Owyhee Mountains in southwestern Idaho. Hydrovolcanic activity decreased and rates of magmatic output decreased (Cummings et al., 2000). The Dry

Creek Buttes fault zone served as a conduit for the last eruptions of calc-alkalic lavas—Double Mountain Rhyolite—in the Oregon-Idaho graben.

3. Local Geology

Cummings (1991b) named the Dry Creek Buttes fault zone for a zone of faults that parallel Lake Owyhee (Figure 4). At the northern extent the 2-3 km wide north-striking Dry Creek Buttes fault zone dissects hydrovolcanic rocks (Tbi), and sandstone, siltstone, and mudstone. In Figure 4, the trap-door structure is situated within the white rectangle; the Burnt Mountain strand is to the east approximately 1.5 km. The two structures deform the sequence of Oxbow Basin.

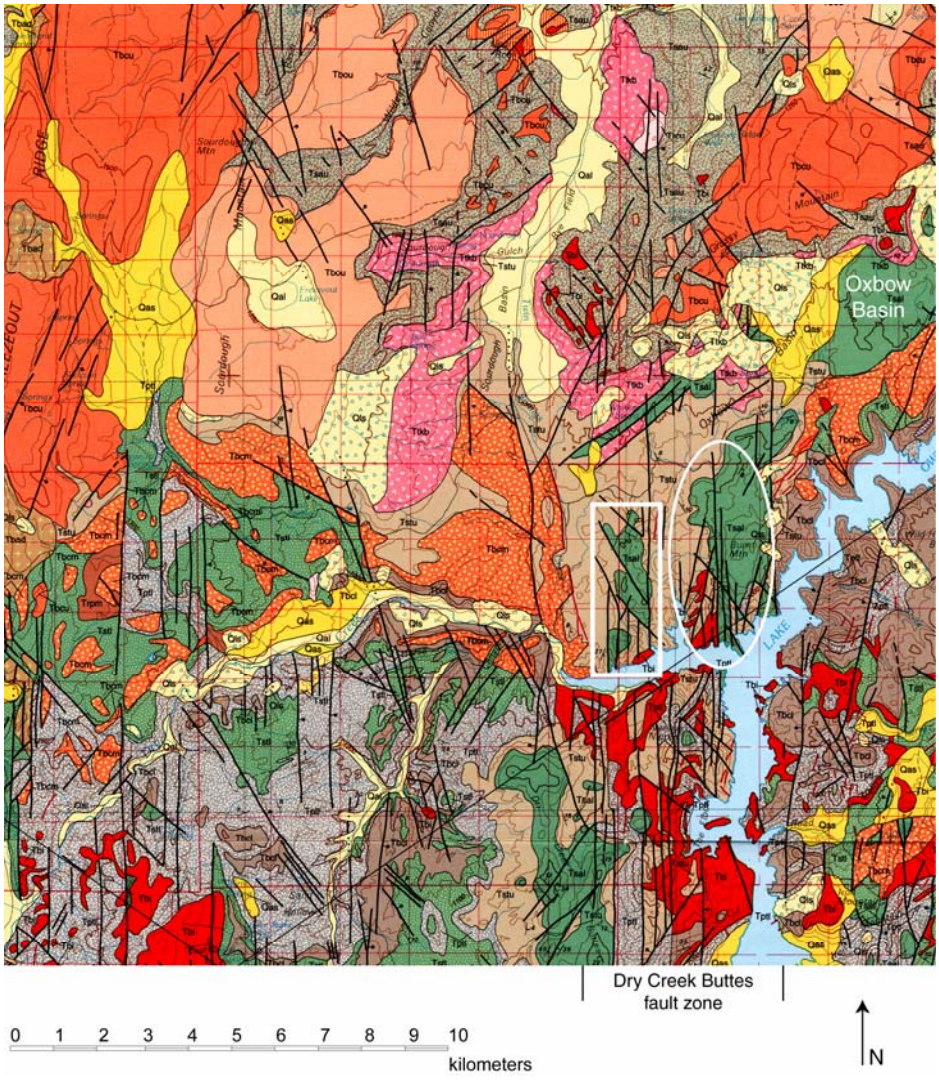

Figure 4. Portion of the 30 x 60 minute geologic map around Lake Owyhee (Ferns et al., 1993). The trap-door structure (white rectangle) is situated along the northwest side of the Dry Creek Buttes fault zone. The Burnt Mountain strand (white ellipse) is 1.5 km east of the trap-door structure. The geographic Oxbow Basin is in the northeast quadrant of the map.

My mapping confirms the stratigraphy of Cummings (1991a) and Ferns and Cummings (1992). I represent the sequence of Oxbow Basin similarly, but divide each component into upper and lower units according to distinct stratigraphic horizons. The remainder of this section, *Local Geology*, is a summary of the structural

evolution of the Dry Creek Buttes fault zone following Hess (1998) and Cummings et al. (2000).

3.1 Structural Evolution of the Dry Creek Buttes Fault Zone

The Dry Creek Buttes fault zone was active throughout the evolution of the Oregon-Idaho graben from 15.5 Ma through subsidence of the western Snake River Plain at about 10.5 Ma (Cummings, 1991a; Ferns et al., 1993; Cummings et al., 2000). The fault zone may reflect a deeper basement fabric, and have served as a conduit for ascending magmas and hydrothermal fluids (Hess, 1998; Cummings et al., 2000) because it is the locus of numerous volcanic centers and hot spring deposits.

NS- and NE-striking fault segments, bedding-plane drag folds, fault-related brecciation, and kink-like folds define the Dry Creek Buttes fault zone (Hess, 1998). Exposed faults are nearly vertical; for that reason, they result in only minor extension. Displacement on the Dry Creek Buttes fault zone influenced sedimentation of the sequence of Oxbow Basin, near Lake Owyhee. As a result, tuffaceous silts, sands, and conglomerates were deposited with some lava flows, and tephra deposits, forming interbeds (Ferns et al., 1993). These deposits comprise the middle Miocene sequence of Oxbow Basin (Cummings, 1991a). The following is a summarized stratigraphic description of Ferns et al., (1993) for the rocks that crop out in the study area:

1. Lower tuffaceous sedimentary rocks, olivine basalt flows, palagonitic tephra, calc-alkaline lava flows, and arkosic sandstones

2. Middle calc-alkaline lava flows, rhyolite and dacite of Dry Creek, basaltic lava flows, tuffs, welded ash-flow tuffs, rhyolite (Jump Creek Rhyolite), and tuffaceous siltstones; and
3. Upper palagonitic tephra, arkosic sandstone conglomerate and post Oregon-Idaho graben tuffaceous siltstone, and calc-alkaline lavas (rhyolite and dacite flows and domes).

3.2 Stratigraphy of the study area

Kittleman et al. (1965) and Kittleman et al. (1967) provide the earliest stratigraphic descriptions of the Deer Butte Formation. Cummings (1991a) revisited the Deer Butte Formation, and described a sequence within the formation that includes a basalt tephra-dominated unit overlain by a sedimentary unit (Table 1). In later descriptions, this sequence is named the sequence of Oxbow Basin (Table 1), where Ferns and Cummings (1992) distinguish separate rock packages into interbedded siltstones and sandstones (Tss_3, Tss_5, Tss_6, and Tss_7); basalt tephra deposits (Tss_1, Tss_4, and Tss_8); and basalt flows (Tss_2). This study involves three rock packages from the sequence of Oxbow Basin, and will they be discussed in more detail in following paragraphs. Table 1 summarizes the succession and evolution of stratigraphic names and use of nomenclature for the study area since descriptions by Kittleman et al. (1965) and Kittleman et al. (1967).

Table 1. A table of descriptions for the sequence of Oxbow Basin.

Cummings, 1991	Ferns et al, 1992	This Study
	Sequence of Oxbow Basin	***Sequence of Oxbow Basin***
SEDIMENTARY UNIT: **Basalt tephra:** Orange-brown; 0-90 m thickness; basalt palagonitic tephra; and Dikes and sills intrude proximal facies. **Lacustrine sediment:** 0-15 m thick; lacustrine siltstone; fish scales; plant fragments; and finely laminated to massive. **Arkose** 0-10 m thick; arkosic; large-scale scour-and-fill cross-bedding; medium-grained to conglomeratic; and muscovite-bearing. **Fluvial sediment** 0-70 m thick; organic-rich siltstone and mudstone, fissile bedded, lignitic seams; and simple channels. ***Stratigraphically equivalent*** Contains fine-grained to granule-size sands and hydrothermally altered silicified clasts. **Lacustrine sediment** 0-60 m thick; light-colored siltstone; finely laminated to massive; plant fragments and fish scales. **Basalt sills** 0-50 m thick; basaltic andesite; brown weathering; massive; locally forms dikes. **BASALT-TEPHRA-DOMINATED UNIT:** **Basalt tephra** 0-100 m thick; basaltic andesite palagonitic tephra; orange-brown; and proximal, intermediate, and distal facies are preserved.	**Tss_8:** Basalt-palagonitic tephra intruded by complex dikes and sills; possible vent-filling basalt flows in diatremes and craters; and fish scales and algal mats.	**Rocks with similar attributes were unobserved**
	Tss_7: Finely laminated to massive siltstones. Fine grained sandstones located north of Dry Creek.	**Rocks with similar attributes were unobserved**
	Tss_6: Coarse-grained arkose: larges-scale scour-and-fill cross-bedding; forms a layer up to 4m thick. Matrix-supported conglomerates: locally contain small pebbles of granite and quartz; algal mats; and fish scales.	**Uppermost** Sandstone (medium-grained) to conglomeratic; light-brown to tan (fresh); dark-red to dark-brown (weathered); arkosic and muscovite-bearing; moderately sorted; very angular to angular, and elongate; Scour-and-fill cross-bedding: local channel lag along foresets.
	Tss_5: Yellow-brown; fine-grained tuffaceous siltstones and sandstones; interbedded lithic rich channel deposits (coarse sandstones); moderately well-rounded; granule to coarse sand; gray to black multiply veined hydrothermally altered silicified clasts; well-sorted sheet sands (north of Dry Creek arm): low-angle cross-bedding, with silicified clasts.	**Middle** Siltstone (approximately 45 m thick); reworked tuffaceous siltstone and claystone; tan to white or buff; interbedded with lenses of sandstone and conglomerate (7.3 m-13.5 m thick). Conglomerate contains black silicified clasts. Sandstone contains plant fossils. Upper contact is conformable with overlying unit.
	Tss_4: Palagonitic tephra deposits; overlie light-to-medium gray organic-rich siltstones. Overlie light-to-medium gray, organic-rich siltstones	**Lowermost** Palagonitic tephra (approximately 35-60 m thick) Dark brown (lower unit) and light brown (upper unit); lower unit is glassy
	Tss_3: Light-to-medium gray; seams of lignite. Contains siltstones with abundant reed fossils; fissile shales; interbedded laminated to massive siltstones. South of Nanny's Nipple, Tss_3 lays conformably on basalt-palagonitic tephra deposits.	**Rocks with similar attributes were unobserved**
	Tss_2: Basalt flows. Thin flows in the southwest corner of the Elbow Quadrangle. May be correlative with the upper flows of Owyhee Basalt.	**Rocks with similar attributes were unobserved**
	Tss_1: Massive basaltic tephra containing blocks of vesicular to massive basalt in a palagonitic matrix. Interbedded with tuffaceous siltstones. Moderately well-bedded tephra deposits contain: palagonitized ash and lapilli; basalt lithic fragments; and accretionary lapilli.	**Rocks with similar attributes were unobserved**

For this study, I follow stratigraphic nomenclature used by Ferns and Cummings (1992) in The Elbow 1:24,000 geologic map. Based on similarities between previous work and my observations, I find that the lowermost, middle, and uppermost rocks in the study area correspond to Tss_4, Tss_5, and Tss_6 of the sequence of Oxbow Basin (Table 1). Figure 5 is a schematic of the sequence of Oxbow Basin; the schematic also includes an interpretation of the units that crop out along the trap-door structure.

3.3 Significant stratigraphic characteristics

A geologic map of the 1:24,000 Elbow quadrangle (Ferns and Cummings, 1992) is the largest scale map and most detailed description of the sequence of Oxbow Basin. This study needed higher resolution descriptions; as a result, I subdivided the existing Tss_4, Tss_5, and Tss_6 into the following units: Tss_4 into units Tss_{4A} and Tss_{4B}; Tss_5 into units Tss_{5A}, Tss_{5B} and Tss_{5C}; and Tss_6 into units Tss_{6A} and Tss_{6B}. The following is a list of distinguishing features of each unit:

- Tss_{4A}: dark brown, glassy, palagonitic hydrovolcanic deposits
- Tss_{4B}: light brown, palagonitic hydrovolcanic deposits
- Tss_{5A}: tan, claystone
- Tss_{5B}: present only on the western slope of the trap-door structure
    - Conglomerate containing black silicified clasts
    - Muscovite-bearing siltstone containing reed fossils
- Tss_{5C}: white, claystone

- Tss_{6A}: tan siltstone
- Tss_{6B}: red-brown muscovite-bearing sandstone

In the remainder of this section I discuss, in more detail, my observations of Tss_4, Tss_5, and Tss_6.

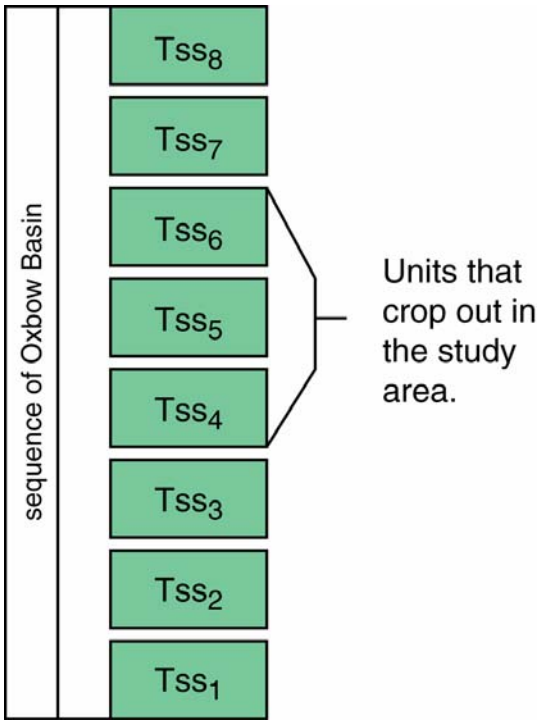

Figure 5. Schematic summary of the sequence of Oxbow Basin (Ferns and Cummings, 1992). This diagram also includes and interpretation of units that crop out along the trap-door structure.

3.3.1 Tss_4

Tss_4, are the lowermost exposed rocks in the study area. Unit Tss_{4A} is dark brown and glassy, and unit Tss_{4B} is brown (Figure 6). The character of the lower contact of Tss_4 is unknown from observations within the study area. Local peperites, however, indicate that Tss_{4A} is directly above an intrusion. On the other hand, the upper contact of Tss_{4B} is sharp and conformable with the bottom of Tss_{5A}.

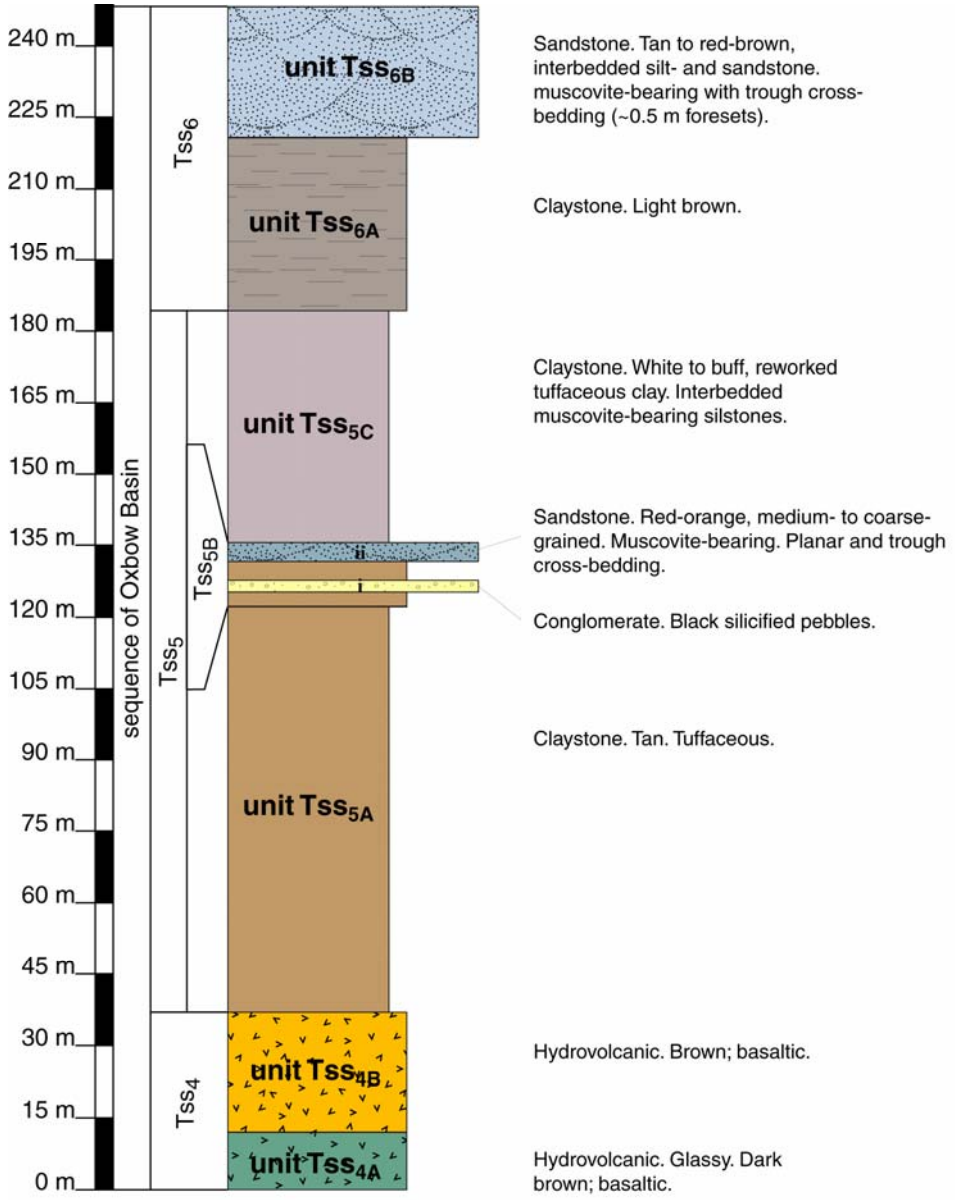

Figure 6. Stratigraphy along the western slope of trap-door structure based on 1:3650 mapping of the study area.

3.3.2 Tss_5

Units Tss_{5A} and Tss_{5C} are tuffaceous silt- and claystone (Figure 6 and Figure 7). Unit Tss_{5A} contains reed fossils when tan, abundant where laminations are purple and green. Unit Tss_{5B} is conglomerate and sandstone (Tss_{5Bi} and Tss_{5Bii}) lenses.

These lenses are diagnostic marker beds, and will be discussed in more detail in following paragraphs. Unit Tss_{5C} is white tuffaceous claystone containing localized muscovite-bearing silt- sandstone lenses (channel deposits). These lenses crop out on the west slope of the study area.

Unit Tss_{5B} is present only on the western slope of the structure (Figure 8). Overall, unit Tss_{5B} includes a conglomerate lens containing black silicified pebbles (Tss_{5Bi}) and a layer of medium- to coarse-grained sandstone (Tss_{5Bii}). They are both dark red to light brown. In most places Tss_{5Bi} is composed of greater than 2 mm framework supported clasts; in other places it is composed of finer grained clasts (less than 2 mm). The coarse grains are present as channel lag in some of the trough cross-stratification. Fine-grained detritus compositions are consistent; Tss_{5Bi} is well-indurated and contains approximately 40% feldspar, 35% lithics (black silicified pebbles), and 25% quartz clasts. Most grains in Tss_{5Bi} are rounded and elongate. The quartz, however, is rounded and equant. Foresets vary from approximately 0.5 m to 1 m long.

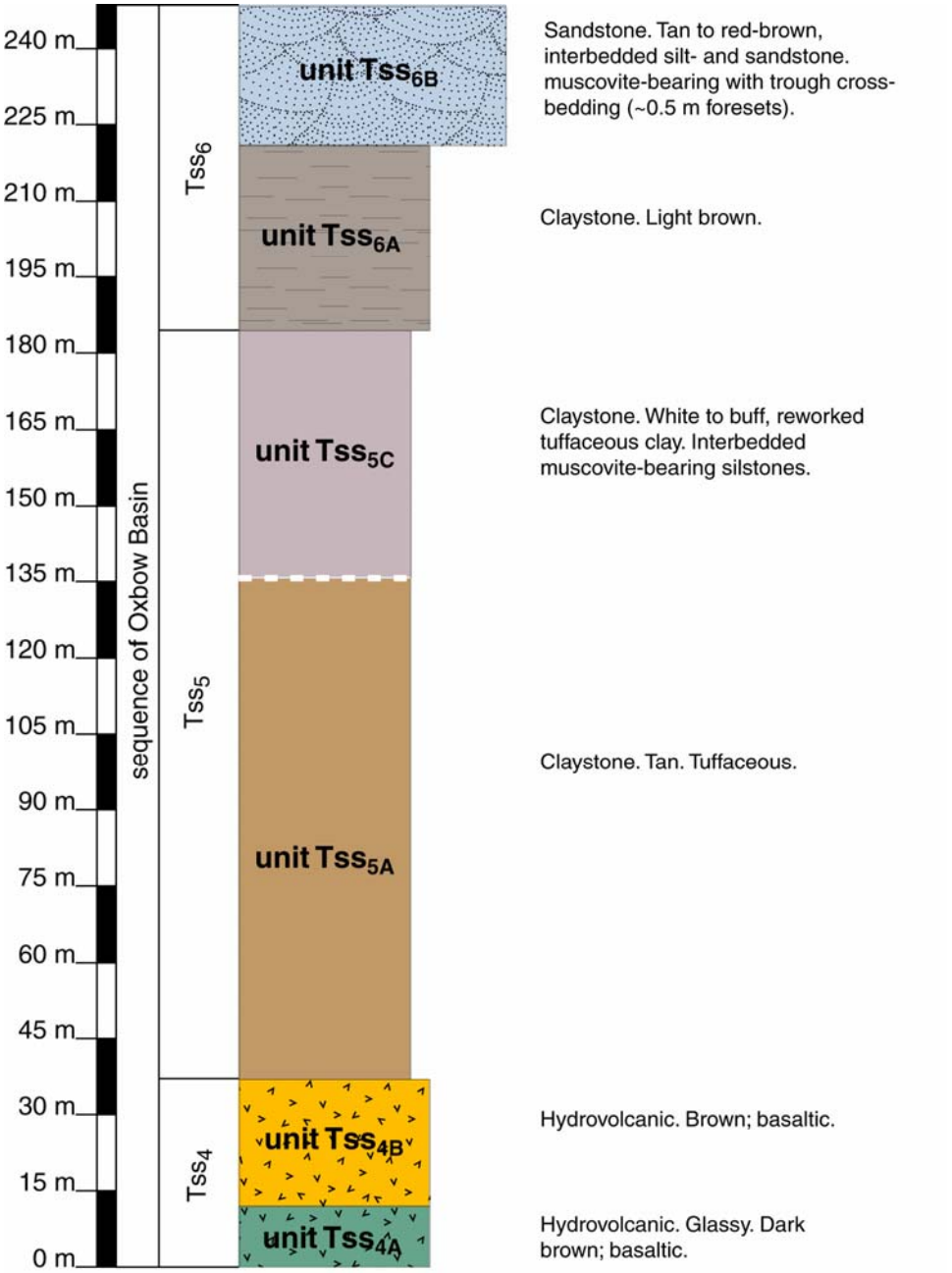

Figure 7. Stratigraphy along the eastern slope of trap-door structure based on 1:3650 mapping of the study area.

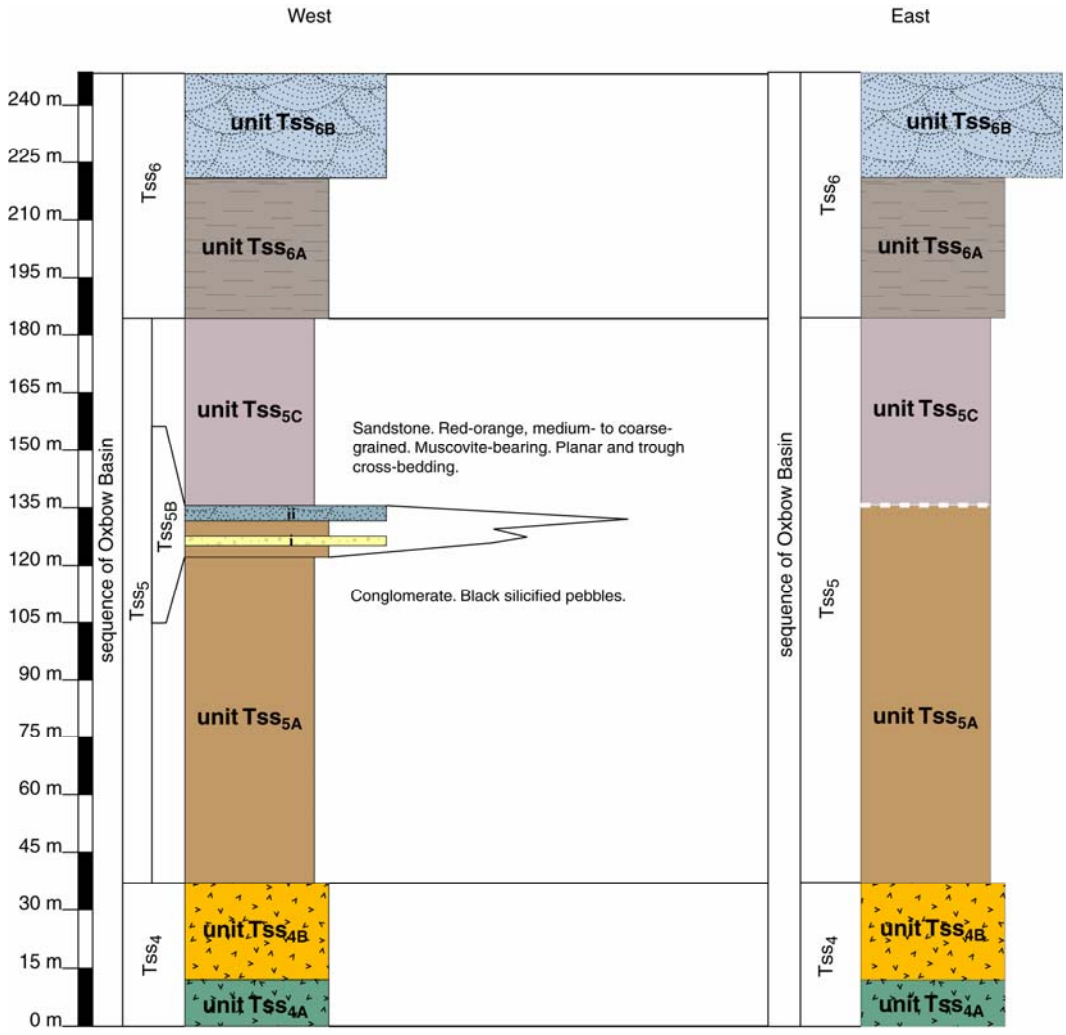

Figure 8. A schematic illustrating the correlation of stratigraphy from west (left) to east (right) in the study area.

Tss_{5Bii} is a lens of tan (fresh) and red-brown (weathered) sandstone (Figure 6). The framework grains are less than 2 mm in diameter, and composed of feldspar, quartz, and lithics—approximately 40%, 30%, and 30%, respectively. The feldspars are rounded and tabular, quartz is equant and rounded, and the muscovite grains are angular and discoidal. There are two bedding geometries: planar (fine-grained) and trough cross-stratification (coarse-grained).

Combined, unit Tss_{5B} is approximately 13.5 m thick to the west and pinches-out to the east (Figure 8). Overall, Tss_5 is consistent in thickness on both sides of the trap-door structure.

3.3.3 Tss_6

Unit Tss_{6A} is light brown to tan (fresh) clay- and siltstone. Unit Tss_{6A} coarsens upward into unit Tss_{6B}. Unit Tss_{6B} is tan (fresh) and dark red to dark brown (weathered) cross-bedded silt- and sandstone, containing 30% white to beige feldspar, 35% quartz, and 35 % muscovite and lithics. The rocks are stained and possibly cemented with hematite. The feldspars are prismatic and rounded; quartz grains are equant and rounded, and the lithics vary in texture from angular with low sphericity. Channel foresets are typically greater than 0.45 m long where channel lag has occasionally been preserved. Plant fossils are present in the fine-grained rocks of the unit, Tss_{6B}. Although Tss_{5Bii} is generally coarser, the presence of muscovite in both, Tss_{6B} and Tss_{5Bii}, indicates a similar provenance.

The thickness of Tss_6 ranges from approximately 40 metres in the northeast to 85 metres in the southwest. Tss_{6B} is a suite of fluvial sediments in sharp conformable contact with the underlying tan silts (14 – 16 m thick) of unit Tss_{6A}.

Figure 9 and

Figure 10 are photographs from the study area demonstrating spatial relationships of the stratigraphic units.

Figure 9. Stratigraphy along the west side of the trap-door structure. Tss_6 varies in thickness, south to north, from 80 m to approximately 40 m. Also, from south to north in this image, the structure extends approximately 1.5 km. The white-dashed lines are faults.

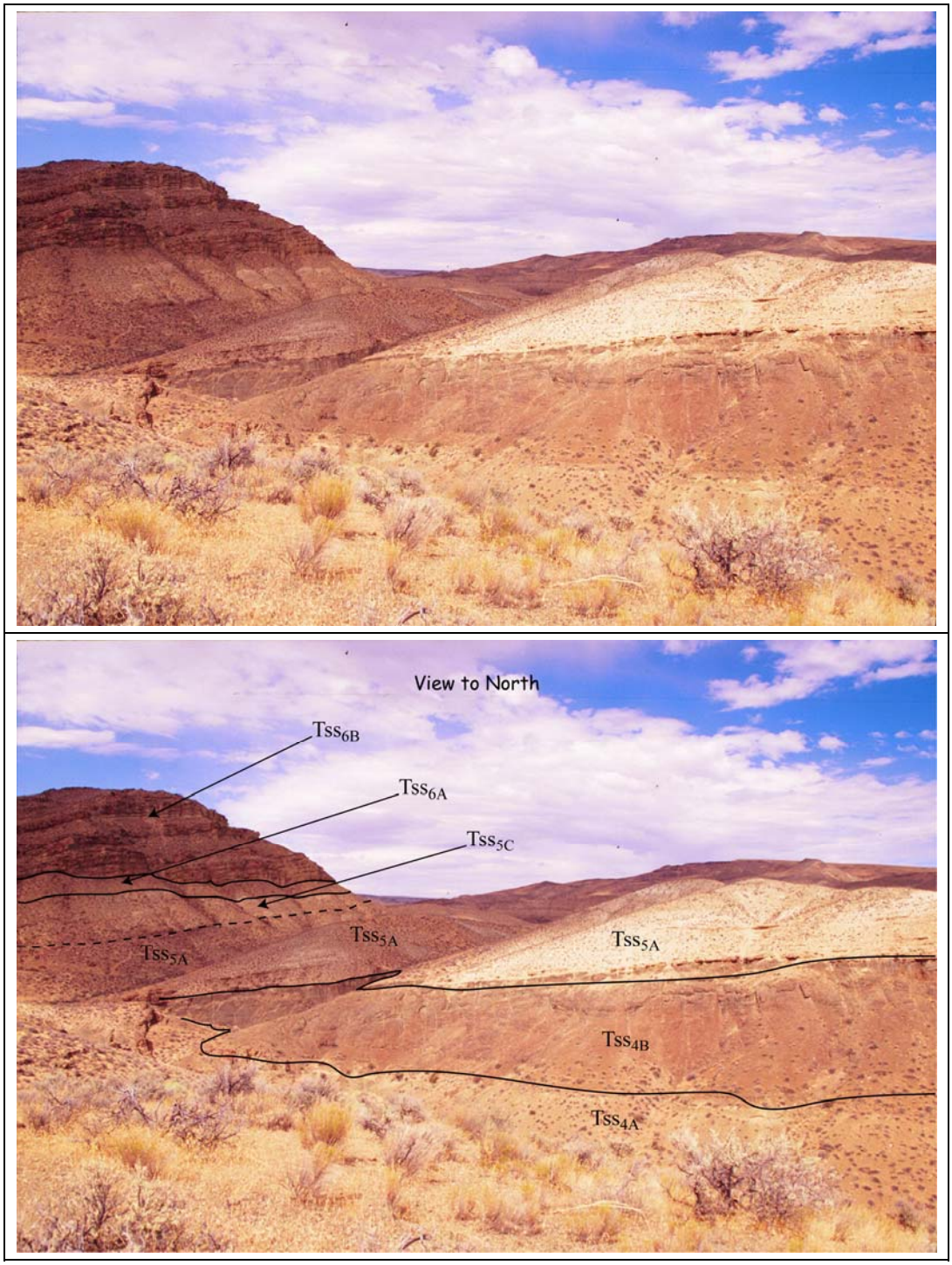

Figure 10. Stratigraphy along the east side of the trap-door structure. Tss_4 is approximately 35 m thick, and the distance from right to left (east to west) is approximately 0.75 km.

4. Geometry of the *Trap-door structure*

Two maps were produced during this study (Appendix A). The first (Appendix A: Plate 1) is an analytic map of features. The analytic map then served as a basis for constructing a geologic map (Appendix A: Plate 2). From the maps, several down-plunge views of the structure were constructed in order to provide details of the variation in the structure along its strike.

The process of describing how the maps were constructed is in the *Methods* section. This description is followed by a discussion on the geometry of the trap-door structure and how various structural fabrics (e.g., joints and deformation bands) are related to the structure and its development.

4.1 Methods

The field investigation lasted 21 days, and occurred in two sessions separated by 7 weeks of map evaluation. Details of layer geometry and structural features were mapped on an enlarged aerial photograph and transferred onto an enlarged portion of the USGS 1:24,000 Twin Springs quadrangle. Bergman Photographic (Portland, Oregon) enlarged aerial photographs from negatives provided by the Bureau of Land Management to a scale of 1:3650. The aerial photograph was the primary base map used for fieldwork.

The study area was traversed on foot and mapped on the enlarged aerial photo (Appendix: Plate 1). The analytic map records the field observations. Where a bed

could be traced, it is marked on the map. In most cases individual beds could not be followed throughout the map area. A group of related beds could be followed, however. It is these groups of beds that are represented on the geologic map. Each solid line on the photo is reproducible and represents features of the rocks that were mapped while traversing the outcrop. The lines show thickness changes and discontinuities. Dashed lines, unless noted otherwise, represent covered or inferred contacts. After completing the field mapping, faults and contacts between stratigraphic units were transposed onto a topographic base map (Appendix A: Plate 2).

The position of the trap-door structure on the enlarged photos is off-center to the southeast quadrant of the print. In order to determine the amount of distortion, I measured the distances between three points whose lengths were the sides of a triangle across the center of the map. The sides were intentionally oriented such that two of them were oriented approximately N-S and E-W. I repeated this on the topographic map. The distortion I measured on the aerial photo is approximately 1% in the N-S direction and 3% in the E-W direction.

After lines were transferred to the topographic base they were checked for geometric consistency with field observations. Map analysis consists of verifying the strike and dip, and stratigraphic thickness of each unit across the map area. Two methods for verifying this information are: two- and three-point problems, and vertical profiles. During the map analysis, I used Rockworks 99 to determine the plunge from observed strike and dips. To make vertical profiles and cross sections, I oriented the

map parallel to the direction of plunge and re-projected the lines into a vertical profile. Using the results, I verified the strikes and dips, stratigraphic thickness, and made cartoons illustrating the geometry of the trap-door structure (Figure 11 and Figure 12).

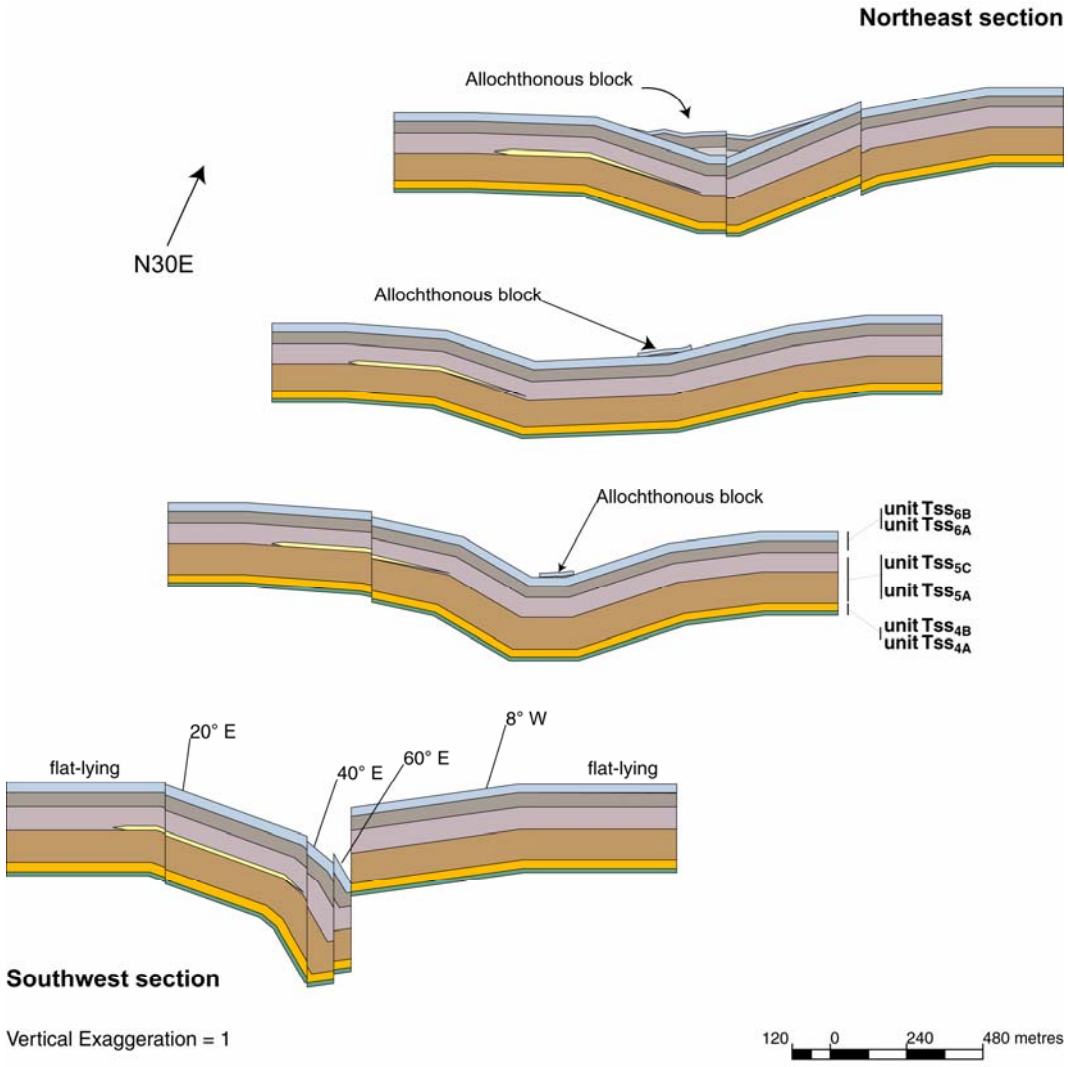

Figure 11. Series of cross-sections based on down-plunge views showing how the faults and shortening relate. Views are from the southwestern extent (Dry Creek) to the northeastern extent. The lens within the western limb represents Tss_{5B}.

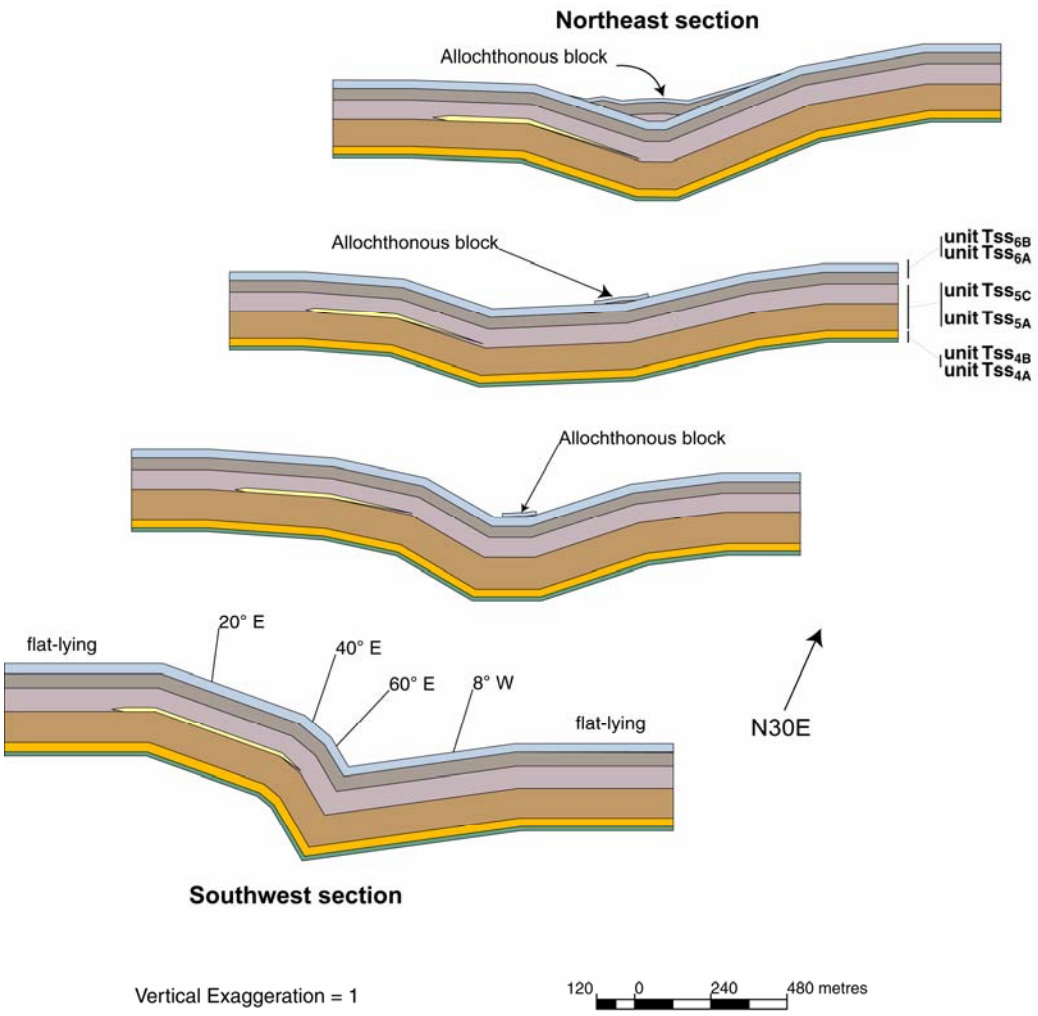

Figure 12. Interpretive view of the trap-door structure. Here, fault displacements have been removed. Views are from the southwestern extent (Dry Creek) to the northeastern extent. The lens within the western limb represents Tss_{5B}.

4.2 Field Observations

During the course of the mapping, the orientation of beds, joints, faults and deformation bands were noted. The orientation of bedding provided the gross geometry of the trap-door structure, while joints and faults and deformation bands and their relationship to bedding provided insights into the relative timing of deformations.

4.2.1 Folding

Tss_4, Tss_5, and Tss_6 of the sequence of Oxbow Basin are the units folded in the study area. The trap-door structure consists of two faulted monoclines, an east-facing monocline in the southwest section, and west-facing monocline in the northeast section. The limbs of the monoclines have relatively consistent dip except in narrow zones where the dip changes rapidly. These zones are interpreted to be kink hinges. Individual kink-fold hinges are zones ranging in width from 2-5 m to approximately 15-20 m. Units change dip (between 8° and 22°) across the kink-fold hinges. Faults are present where bedding dip changes take place. Additionally, the amplitudes of the monoclines and kinks remained unchanged up-section (Figure 11).

The kink-fold hinge-width and dip varies from northeast to southwest. For example, the northeast section of the trap-door structure has subtle dip changes relative to the southwest section. The deformation occurs along two, *en echelon* monoclinal fold limbs. The sequence of limb dip angles from west to east (Figure 11) at the southwestern view is: (1) flat-lying, (2) 20° east, (3) 40° east, (4) 60° east, (5) 8° west, and (6) flat-lying, where the east half is structurally lower than the west. However, the sequence of limb dip angles from west to east at the northeastern view is: (1) flat-lying; (2) 2° east; (3) 18° east; (4) flat-lying; (5) 22° west; (6) 10° west; and (7) flat-lying; where the eastern half is structurally higher than the west (Figure 11). The western portion of the structure seems to die out to the north, while the eastern portion grows (Figure 13).

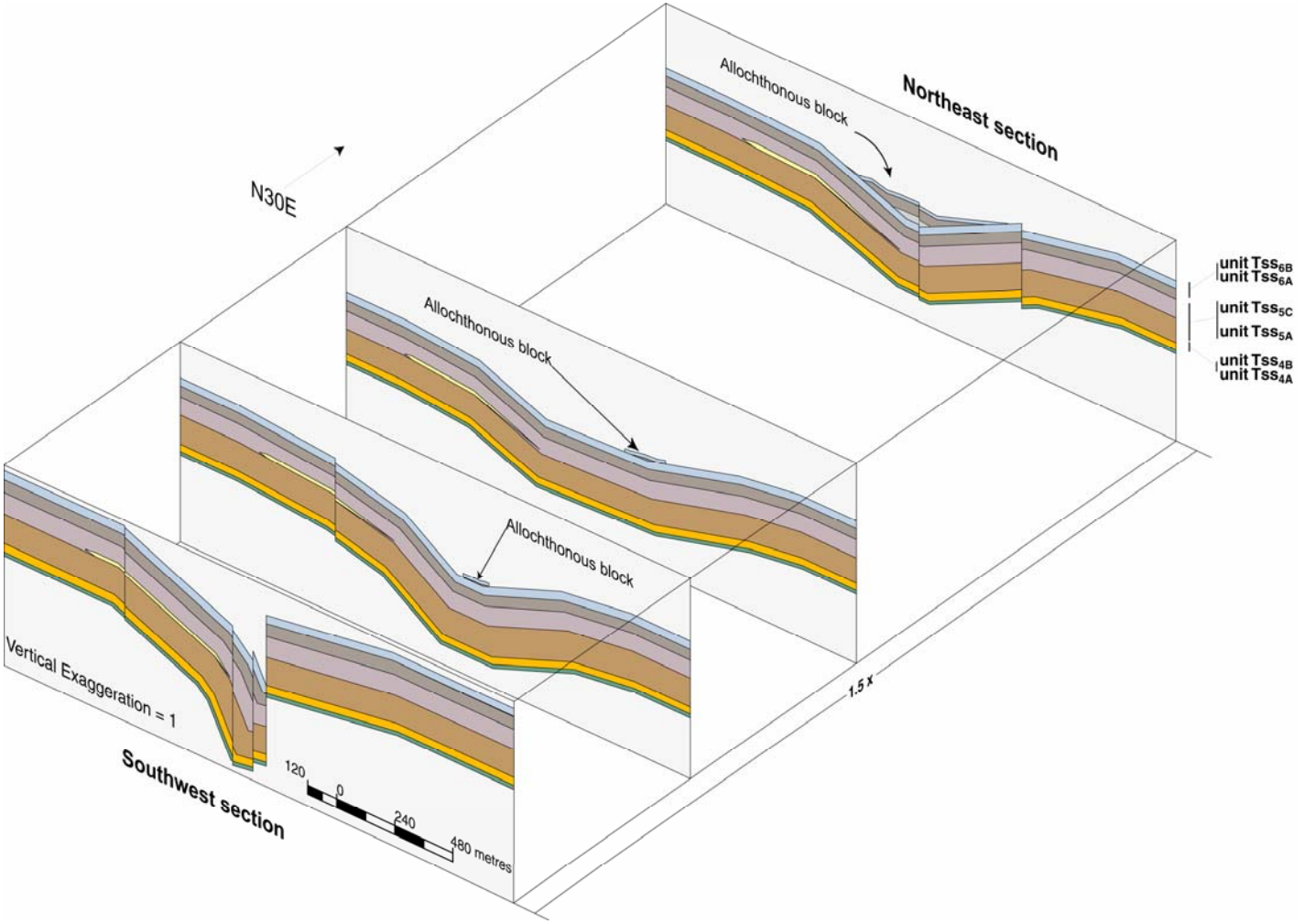

Figure 13. A three-dimensional view of the structures sets the kinks in context from southwest to northeast. The lens within the western limb represents Tss_{5B}.

4.2.2 Deformation Bands

Deformation bands are shear zones (Johnson, 1995) that, in the study area, are present near and parallel to faults. As a result, they represent vertical shear. It appears as if many of the faults initiated as zones of deformation bands. This observation confirms the work of Aydin and Johnson (1978); Aydin and Johnson (1983), and Antonellini et al., 1994). In the study area, NE and N-NW oriented deformation bands have been found in areas of low joint density on Tss_6 and Tss_{5b}. The deformation bands rarely show offset. Deformation bands coincide with regions of dip change and were observed in the following locations: (1) on the west side in Tss_{5Bi} and Tss_{5Bii}, (2) in Tss_{6B} on the north and south ends of the structure, and (3) in the topographic low between the north and south ends of the structure, in Tss_{5Bii}. Deformation bands, however, are not restricted to sandstone layers; Tss_{5Bi} contains them ranging greater than 1 cm to less than 4 cm wide. This is the first report of deformation bands in conglomerate.

Although sense of displacement is unknown, the deformation bands are offset wherever they are preserved in Tss_{5B}. Offsets range from centimetres to a metre or more (faults). Where offset motion could be determined, the displacement was primarily dip-slip. A component of strike-slip motion was apparent, however, it was less than 4% of the overall motion. No motion indicators were found on deformation bands with small (less than 1 m) displacements.

4.2.3 Faults

Faults on the trap-door structure that have displacement greater than 2 m are located near kink-fold hinges, (Figure 11). These faults are vertical in the units exposed. The orientations on the kink-hinges, and faults, are NNE in the northeast section and NNW in the southwest section.

Allochthonous blocks that are present in the fold axes appear on the cross sections. (Figure 11). The allochthonous blocks could be interpreted as accommodations to shortening prior to folding or gravity slides from adjacent regions, like Burnt Mountain to the east, prior to folding.

4.2.4 Joints

Joints have been found in the coarse-grained units (interbeds of Tss_5 and Tss_6) in nearly every outcrop. Joint density varies. In areas where faulting was observed, joint density (joints per metre, jpm) was relatively high (10 ± 2 jpm,). However, high joint density was also observed in areas lacking faults. Such locations tend to be at or near the kink axes. In areas of consistent dip, lower joint densities are on the order from 0.1 jpm to 2 jpm. Orientations on the joints were observed to change with changes in bedding plane orientations, but the angle between joints showed little (approximately 5°) change.

Structural Interpretation of the Joints

Cruikshank and Aydin (1995) show that joint patterns can record the evolution of a stress regime. Since locally, only one orientation of joints can form at a time more than one orientation of joints within a unit testifies to the pattern of its evolution (Cruikshank and Aydin, 1995). The joints on the trap-door structure are planes oriented to both the NW and NNE. Consistency of angles between the joints and bedding planes has implications for the timing of earliest deformation in the study area. The fact that the folding rotates the joint orientations suggests the joints were there prior to the folding. In fact, the relative orientations and timing on the NW joints is evidence that the principal compression orientation evolved from NNE to NW. Eventually, the compression evolved to an EW orientation, which is responsible for the folding. Consistent with observations in the field, the NW-oriented joints are younger than NNE-oriented joints (Cruikshank and Aydin, 1995).

Nowhere did I find joints cross-cutting deformation bands; therefore, the temporal relationship between joints and deformation bands was undetermined. However, since most of the deformation bands have been displaced by faults, it may be concluded that the deformation bands are older than the faults.

4.3 Kinematic Evolution

Joints are mode-one fractures so they form normal to the minimum principal stress (e.g., Cruikshank and Aydin, 1995). The joint patterns on the trap-door structure formed from localized stress that was initially oriented NNE. This produced

joints, but no folding. Subsequently, joints indicate that stress evolved parallel to NNW. Finally, the local stress field migrated parallel to NW. At some time prior to folding, layer-parallel shortening produced an allochthonous block repeating a portion of Tss_5 and all of Tss_6. Folding resulted in the current geometry. Since deformation bands are compressional features, they may have formed during folding, or after folding and prior to faulting. Once the fold axes (shear zones) were established, the faults began propagating and displaced the local stratigraphy. The current geometry is shown in Figure 13.

5. Mechanical Model

Given the observations in this study, and other studies in the Oregon-Idaho graben, two related processes may be responsible for the trap-door structure geometry. They are (1) localized deformation above the margins of sill-like intrusions, and (2) deformation above the tip of a buried fault. Given the regional nature of the intragraben fault zones, buried faults are the more likely explanation. This mechanism will be the focus of my analysis. This section is intended to:

1. Illustrate the geometric and mechanical components used by the Purdue Faux-Pli Forced Fold numerical model (Johnson and Johnson, 2002),
2. Summarize the mechanical theory for deformation above a buried fault, and
3. Present empirical results from a series of numerical trials related to the trap-door structure geometry.

A family of solutions based on this model is presented in the *Discussion* section.

5.1 Mechanical Theory

Most of the assumptions for this study are inherited from the boundary conditions for the model, which is based on the mathematical descriptions of deformation of a sedimentary cover over basement faults developed by Patton and Fletcher (1995, 1998). There are six assumptions for the model, summarized from Patton and Fletcher (1995, 1998), and Johnson and Johnson (2002), they are:

1. A sequence of layers in the sedimentary cover can be modeled as a single linear viscous layer with some degree of anisotropy;
2. Stress and deformation in an anisotropic body can be approximated by a solution for rigid-block motion at its base;
3. Modeling the basement-overburden contact as a thin viscous film emulates the real behavior of the contact. By varying the film viscosity, the contact can range from non-slip (i.e. bonded or welded contact) to freely slipping;
4. The velocity, or displacement, imposed at the base of the layer is precisely equal to the relative motion of rigid blocks;
5. The upper surface of the layer is a traction-free planar surface. Therefore, the stresses are equal to zero in the solution; and
6. The velocities at the upper surface are zero.

5.1.1 Geometry of the Strain

The mechanical analysis of the trap-door structure is simplified to three two-dimensional problems. For an incompressible fluid under constant pressure, $\frac{\partial P}{\partial x} = 0$, the two normal stresses, σ_x and σ_z, and the shear stress τ_{xz}, can be written in terms of a stream function ψ(x,z):

$$\sigma_x = \frac{\partial^2 \psi}{\partial z^2},\ \sigma_z = \frac{\partial^2 \psi}{\partial x^2}, \text{ and } \tau_{xz} = \frac{\partial^2 \psi}{\partial x \partial z} \qquad (1.\ 1)$$

in a Cartesian coordinate system.

$$\nabla_1^2(\nabla_1^2)\psi = 0 \text{, or } \nabla_1^4\psi = 0 \qquad (1.\ 2)$$

In expanded form the equation is:

$$\frac{\partial^4\psi}{\partial x^4} + 2\frac{\partial^4\psi}{\partial x^2 y^2} + \frac{\partial^4\psi}{\partial y^4} = 0 \qquad (1.\ 3)$$

The biharmonic equation is solved using perturbation methods. That is, the total displacement of material points in the sedimentary cover is the sum of the displacements resulting from the uniform movement of the basement (the mean flow), plus the relative motion of points in the basement (the perturbed flow). The perturbed flow of the basement-sediment interface causes the interface to have a non-planar shape. A Fourier series approximation to the shape of the interface is computationally efficient. Therefore, a finite Fourier series of the form:

$$w(x,0) = \sum_{n=1}^{N} V_n \sin(n\lambda x) \qquad (1.\ 4)$$

is used, where λ is the wavelength and *w* is the displacement in the z direction. The specific Fourier series for a fault-step shape is (Patton and Fletcher, 1995):

$$V'_n = V\cos\delta(4/n\pi)\Gamma_n \qquad n = 1, 3, 5, 7\ldots.$$

Where δ represents the dip of the fault. The Gibbs factor, Γ, where

$$\Gamma_n = [\sin(n\pi/(N+1))]/[n\pi/(N+1)] \qquad (1.\ 5)$$

improves the smoothness and convergence of the Fourier series approximation (Hamming, 1973; Lanczos, 1961; Patton and Fletcher, 1995).

For the horizontal velocity components:

$$u(x,0) = \sum_{n=1}^{N} V'_n \sin(n\lambda x) \quad \text{(Patton and Fletcher, 1995)} \qquad (1.\ 6)$$

A function that satisfies the biharmonic equation for vertical motion where the above Fourier series describes the interface shape is:

$$\psi^{(v)}(x,z) = +\sum_{n=1}^{N} [1/(n\lambda)]\{[A_n + B_n(n\lambda z - 1)]e^{n\lambda z}$$

$$+ [C_n + D_n(n\lambda z + 1)]e^{-n\lambda z}\}\cos(n\lambda z) \qquad (1.\ 7)$$

(Patton and Fletcher, 1995), where $\lambda = 2\pi/L$. A_n, B_n, C_n, and D_n are undetermined coefficients. The solution for the coefficients depends on the applied boundary conditions. There is a set of *n* coefficients, one for each component of the Fourier series used to represent the basement-cover interface. It is these coefficients that the solution method solves for. For the horizontal component of motion:

$$\psi^{(h)}(x,z) = -2\eta\sum_{n=1}^{N} [1/(n\lambda)]\{[A'_n + B'_n(n\lambda z - 1)]e^{n\lambda z}$$

$$+ [C'_n + D'_n(n\lambda z + 1)]e^{-n\lambda z}\}\cos(n\lambda z) \qquad (1.\ 8)$$

(Hamming, 1973; Lanczos, 1961; Patton and Fletcher, 1995). Since these functions satisfy the biharmonic equation they are solutions for the trap-door structure and its boundary conditions.

5.1.2 Boundary Conditions

Each term in the solution has four undetermined coefficients. Thus, four boundary conditions are required in order to solve these equations. The boundary conditions illustrated in Figure 14 vary depending on the exact formulation of the model, however, a combination of the following conditions provides a sufficient number of conditions to solve the boundary value problem posed above (Patton and Fletcher, 1995):

1. Motion of the fault blocks to either side of a fault, at over one wavelength from the fault (L) is constant.
2. The upper surface is traction free.
3. Normal displacements at the basement-overburden contact are the same for both the basement and overburden materials.
4. For a bonded basement-overburden contact, shear displacements at the basement-overburden contact are the same for both the basement and overburden materials for bonded contacts.
5. For a frictional basement-overburden contact, shear displacements at the contact can vary in a specified manner.
6. For a freely slipping basement-overburden contact, shear stresses are zero.

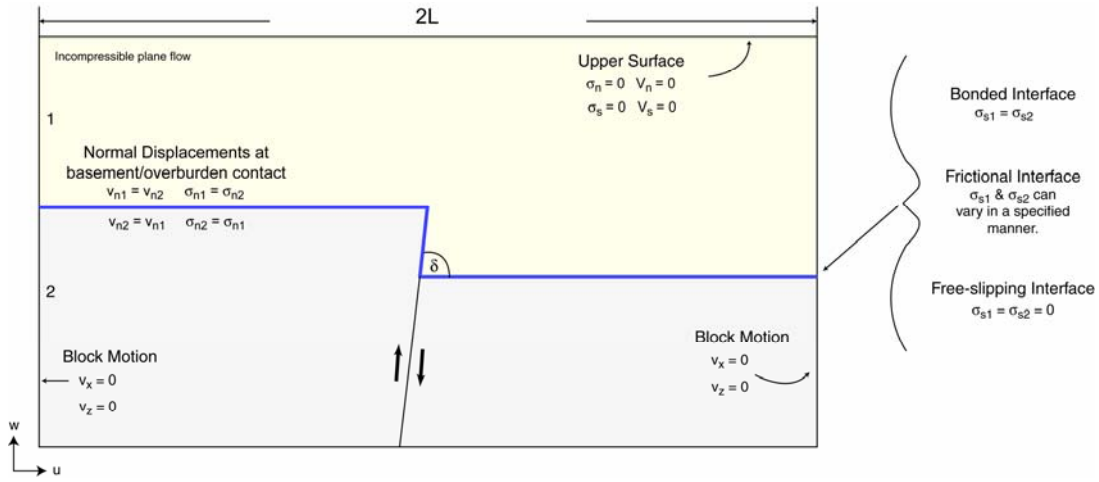

Figure 14. Boundary conditions for the Faux-Pli Forced Fold mechanical model.

5.1.3 Material Properties

Material properties of the lithologic units enter the solution via a series of material coefficients. For elastic materials, the biharmonic equation becomes

$$\frac{\partial^4 \Phi}{\partial x^4} + 2\left(\frac{v}{1-v}\right)\frac{\partial^4 \Phi}{\partial x^2 y^2} + \frac{\partial^4 \Phi}{\partial y^4} = 0 \qquad (1.\ 9)$$

where v is Poisson's ratio. For single-layered viscous material, the biharmonic equation becomes

$$\frac{\partial^4 \psi}{\partial x^4} + 2\left(\frac{\mu_n}{\mu_s}\right)\frac{\partial^4 \psi}{\partial x^2 y^2} + \frac{\partial^4 \psi}{\partial y^4} = 0 \qquad (1.\ 10)$$

where μ_n represents viscosity normal to direction of principal strain, and μ_s is the shear viscosity (Johnson and Johnson, 2002).

The theory is formulated for a single viscous layer but can be used in a multi-layer case by including an anisotropy, (μ_n/μ_s), (Johnson and Johnson, 2002). An

anisotropic medium is a heterogeneous medium, and deforms differently in any particular direction (Johnson and Johnson, 2002; Lekhnitskii, 1981).

5.2 Purdue Faux-Pli Forced Fold Numerical Model

The Purdue Faux-Pli Forced Fold numerical model (Johnson and Johnson, 2002) is a mathematical block-motion solution for deformation of a layer above a buried fault of arbitrary dip and sense of slip (Patton and Fletcher, 1995). Figure 15 shows the components required by the Purdue Faux-Pli Forced Fold mechanical model: fault depth; fault dip; total fault displacement; sense of slip; fault plane geometry (curved/straight); degree of anisotropy; and behavior of the basement-overburden contact (free-slip to welded). By definition of incompressibility, the model conserves mass and volume.

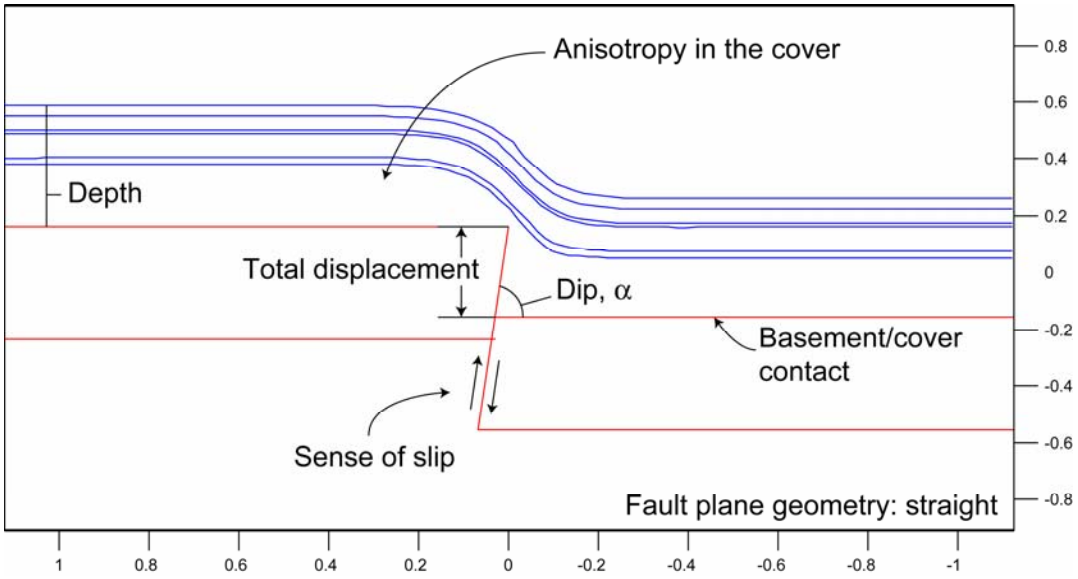

Figure 15. This diagram illustrates the different components used by the Purdue Faux-Pli Forced Fold (Johnson and Johnson, 2002) numerical model.

5.3 Outline of Model Solution

Once the user has entered the appropriate geometric and rheological properties, the Purdue Faux-Pli Forced Fold numerical model solves the biharmonic equation for the unknown variables by integration. For each interval in the integration, the geometry of strain changes. These changes in strain geometry must be incorporated into the next integration step; this is accomplished by Runge-Kutta integration through time.

The Purdue Faux-Pli Forced Fold numerical model allows the user to specify the integration step-size and number of terms in the finite Fourier series. The **Mode of calculation** user interface is the avenue by which the user specifies the step-size and number of terms. The user chooses **preview** or **final**, which specifies the integration-step size. Option **final** sets the program to integrate the biharmonic equation at smaller intervals, reducing geometric errors in the solution. These small step-sizes become computationally expensive; **preview** offers a less computationally expensive step-size with good results for this study. In addition, the user specifies the number of terms in the Fourier series by adjusting the slider bar. Figure 15 and the solutions in the *Model Results* and *Discussion* sections are results from integration in the preview mode for more than thirty terms (approximately 1 minute) in the Fourier series.

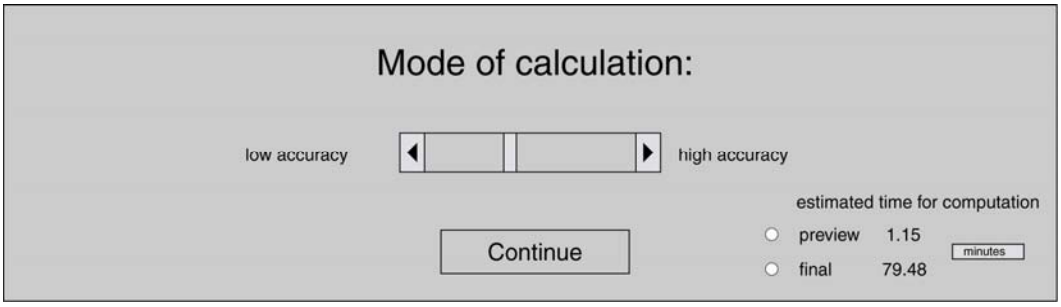

Figure 16. Example of how user prescribes the integration step-size and number of terms in Fourier series.

5.4 Model Results

Folds that develop from the vertical displacement of a buried feature, such as a faults or igneous intrusions, are called forced folds. It is reasonable to expect that the fold geometry is related to the geometry and depth of the buried feature. For example, displacements on buried faults deform the overburden producing a fold like that in Figure 15. Here, I explore three parameters that affect fold geometry using the Purdue Faux-Pli Forced Fold numerical model. The three parameters are fault geometry and displacement, anisotropy of non-faulted overburden, and behavior of the basement-overburden contact (free-slip or bonded).

The goal is to identify the subsurface structures most likely responsible for the structures mapped at the surface. The essential fold geometry is captured by three attributes: fold amplitude; fold width; and the dip of the center portion of the kink. Using a ruler and protractor, I physically measured the three attributes from the graphical output of the model. The model automatically scales the graphic such that vertical exaggeration is always equal to one; as a result, the folds become small compared to the depth of the fault. Consequently, interpretations become more

sensitive to measurement as fault depth increases. Figure 17 and Figure 18 are charts produced from the measurements I made. Figure 18 shows the scatter from my measurements. There is more scatter for deeper faults. Thus, interpretations become less reliable for deeper faults.

5.4.1 Effect of Fault Geometry and Displacement

Four fault geometries are considered—straight normal, straight reverse, curved (listric) normal, and curved (listric) reverse. Ideally, a straight fault has a planar surface and a listric fault has a curvilinear surface, where normal and reverse indicates the sense of displacement. Fault type largely controls the vertical displacement of the overburden.

The boundary conditions imposed on the general solution require that in the specific solution there is a one-to-one linear relationship between the fault throw and the vertical displacement on the fold (Johnson and Johnson, 2002; Patton and Fletcher, 1995) (Figure 17). Thus, the amplitude of the modeled trap-door structure directly reflects the throw on the underlying basement fault.

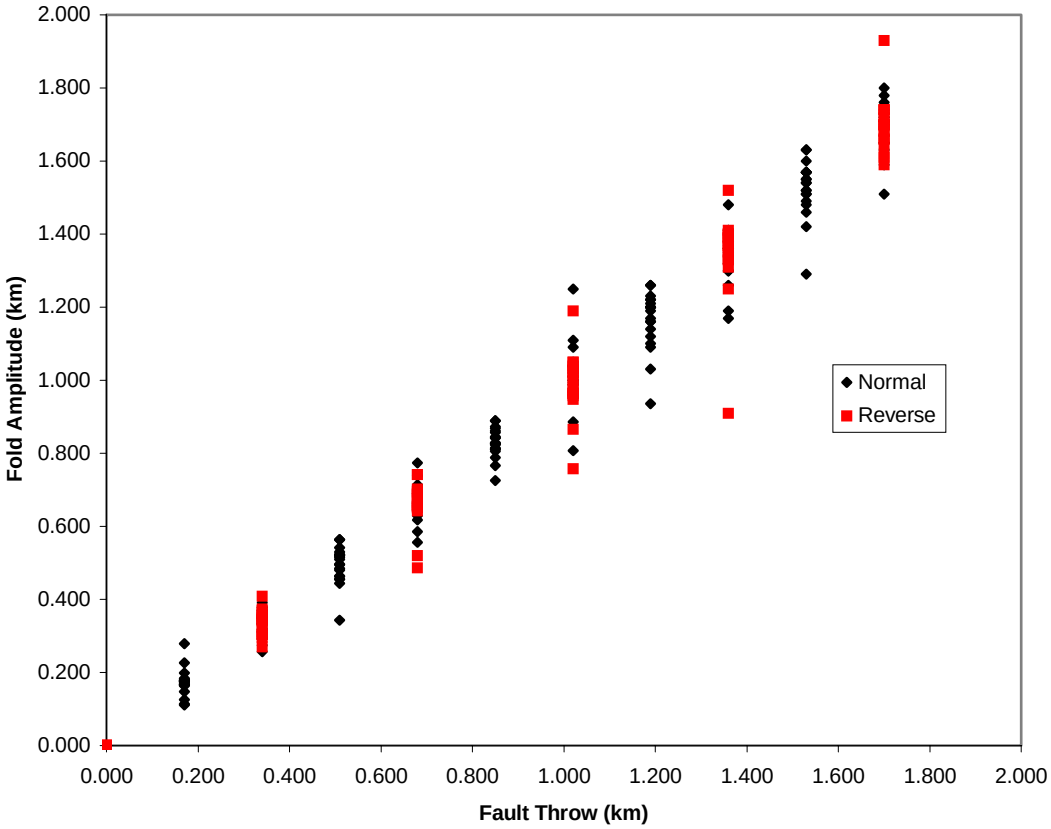

Figure 17. The modeled relationship between fold amplitude and fault throw on buried straight faults between angles 45° and 90°. The diamonds are normal faults, while the squares are faults.

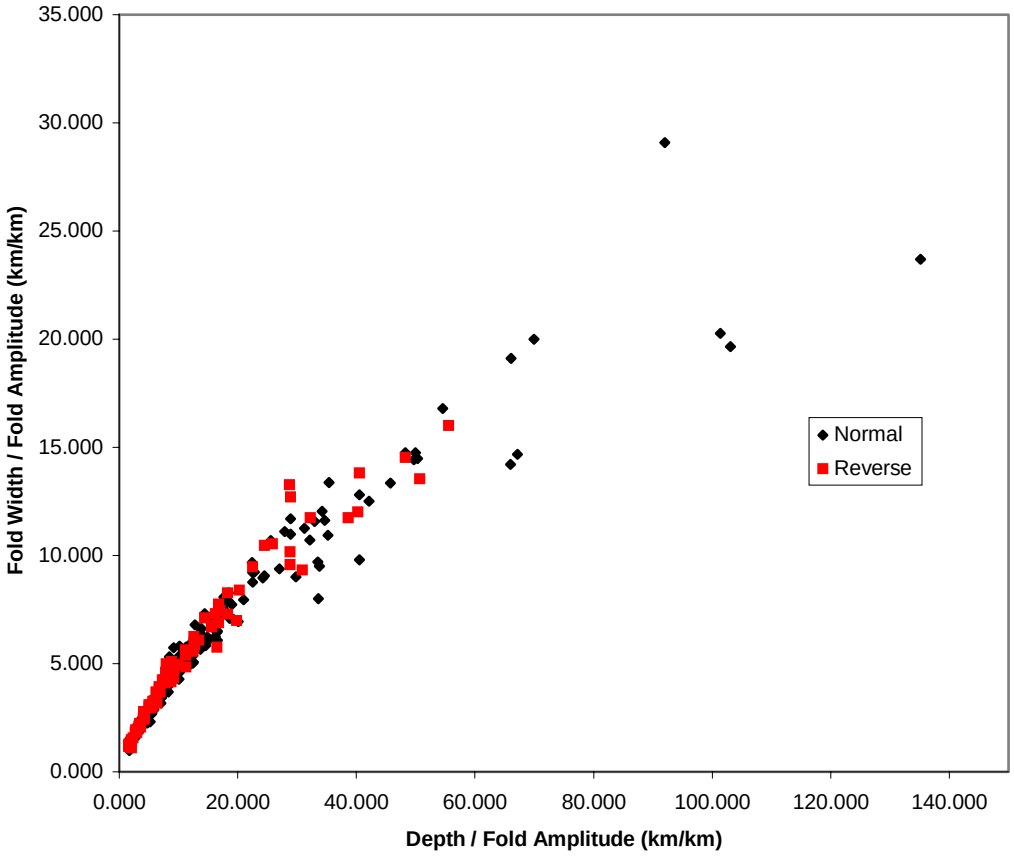

Figure 18. The modeled relationship between the geometry of a kink-like fold and the geometry and orientation on buried straight faults between angles 45° and 90°. The diamonds are normal faults, and the squares are faults.

Figure 18 confirms that a straight reverse fault will produce the same fold amplitude as a straight normal fault of opposite dip. This result is not particularly enlightening because 1) the overburden feels only the direction of displacement, not the geometry of the buried structure, and 2) the solutions for normal and faults are the same in the model, only opposite in sign. Thus, the model must not be used to infer the sense of slip or direction of dip on a buried straight fault. The sense of displacement and dip direction must be determined, or deduced, by geological

observations during field mapping. Faults within the Dry Creek Buttes fault zone are essentially vertical – measured dips are in the 85-90° range. The stratigraphy gives the sense of displacement of down-to-the-east. The evolution of joint orientations and presence of early stage allochthonous blocks indicate E-W shortening, so one would expect reverse displacements on a buried fault.

A curved basement fault (Figure 19) produces an asymmetric anticline in the overburden. Shortening occurs in two places, above the fault tip, and at the opposite end of the up-thrown fault block. Rotation of the overburden occurs above the rotated fault block. The amount of rotation depends on the length of the rotated block, fault dip, and curvature of the fault plane. Curved faults that produce little rotation (< 5°) must either obey the following approximate relation:

$$0.0872 > \frac{d}{L}$$

where 0.0872 is the sin (5°), d is the throw and L is the length of the rotated block, or have a small amount of curvature. The first case requires a great amount of space for faults showing appreciable vertical displacement. In the second case, the curved fault geometry approaches that of a straight fault. The mapped trap-door structure is a narrow band of deformation like that at the modeled fault-tip (Figure 19), but has horizontal layers to the immediate east and west. Thus, it is unlikely that the trap-door structure is above the tip of a curved fault.

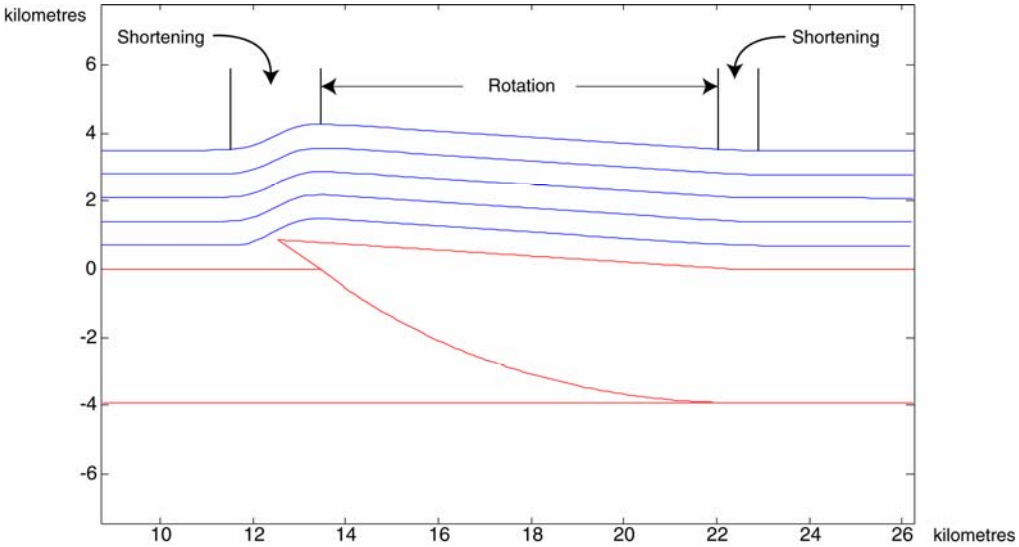

Figure 19. This diagram shows the fold geometry that a curved reverse fault would produce. There are two zones of shortening and a zone of rotation.

5.4.2 Effect of Anisotropy

The degree of anisotropy in the overburden and the character of the basement-overburden contact primarily influence fold width. Increased anisotropy increases the steepness of fold limbs. In order to investigate the sensitivity of fold width and steepness to anisotropy, I ran a sequence of model simulations. In Figure 20 there is a transition in the importance of anisotropy on fold width. It is marked with the black, solid and dotted lines at the area where the slope becomes close to zero. To the left of the line, anisotropy controls the fold geometry. To the right, anisotropy has little to no effect on fold geometry. Anisotropy effects fold geometry equally above reverse and normal faults, as indicated by experiments on a 2.75 km deep fault. The sensitivity of fold steepness to anisotropy increases with fault depth (Figure 21).

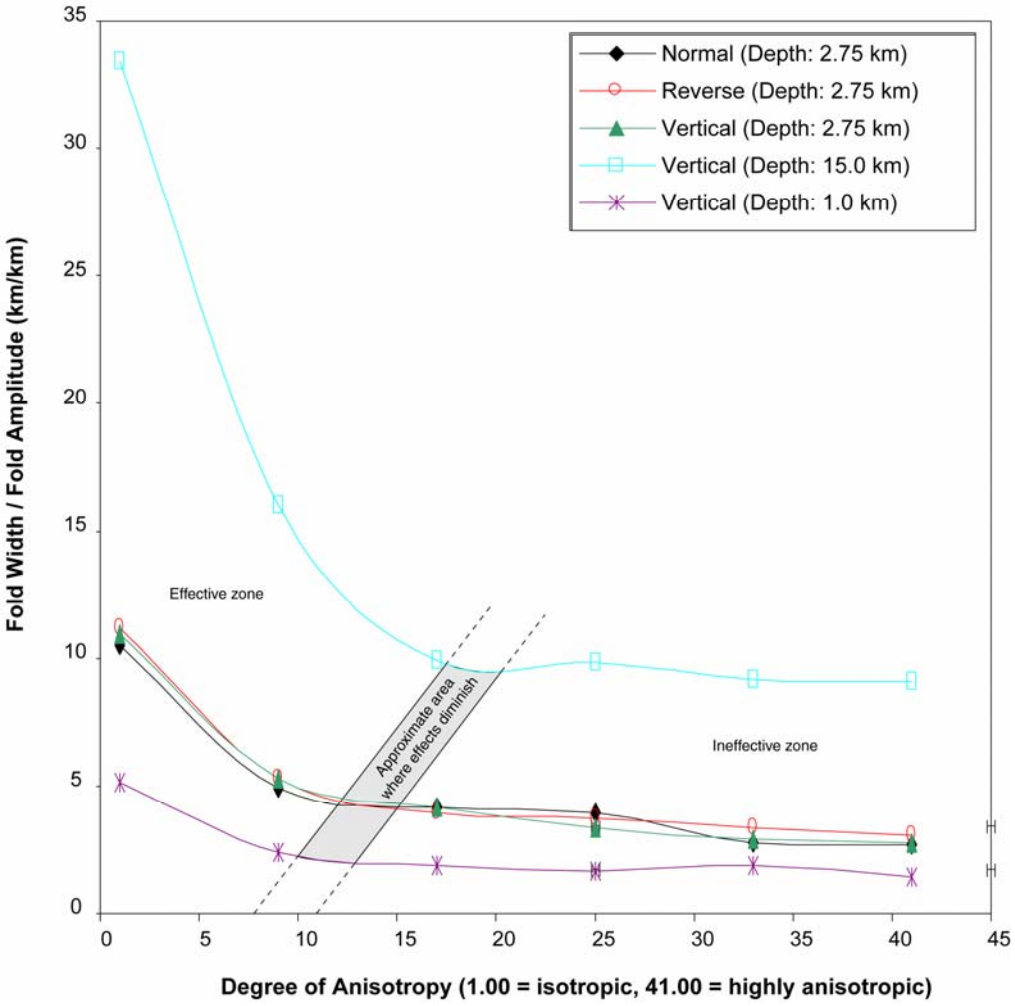

Figure 20. Anisotropy affects the geometry of deformation for a particular range. The model experiments represented here show that the effective zone is narrow at small fault depths compared to large fault depths.

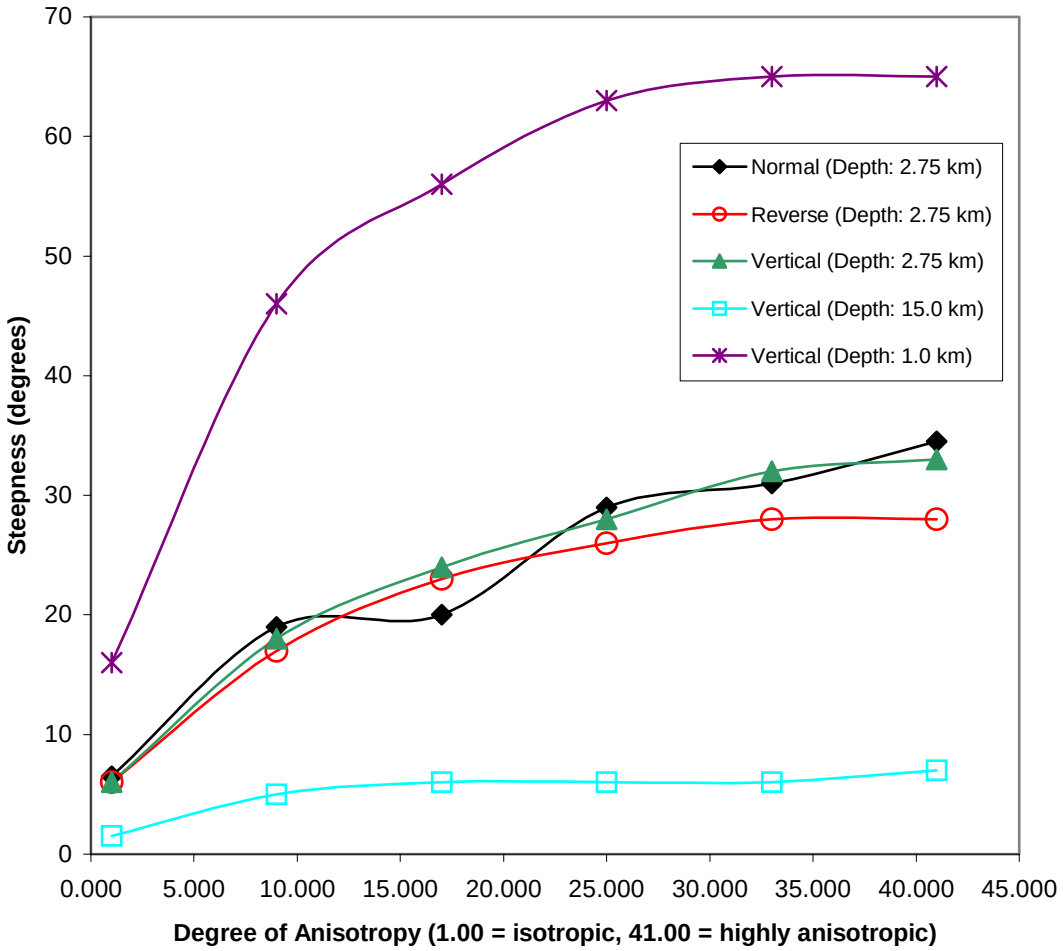

Figure 21. Model experiments show that fold limb steepness is more sensitive to anisotropy at large fault depths than small fault depths.

5.4.3 Effect of Basement-Overburden Contact Properties

The behavior of the basement-overburden contact describes relative motion between the basement and cover, and affects the rate at which the perturbation in the cover grows. In Figure 22 it appears that the behavior of the contact between the basement and cover varies significantly with fault-tip depth, especially at large depths.

However, the predictions for large fault depths are more sensitive to measurement errors. As a result, the effect may be an artifact of my measurement technique.

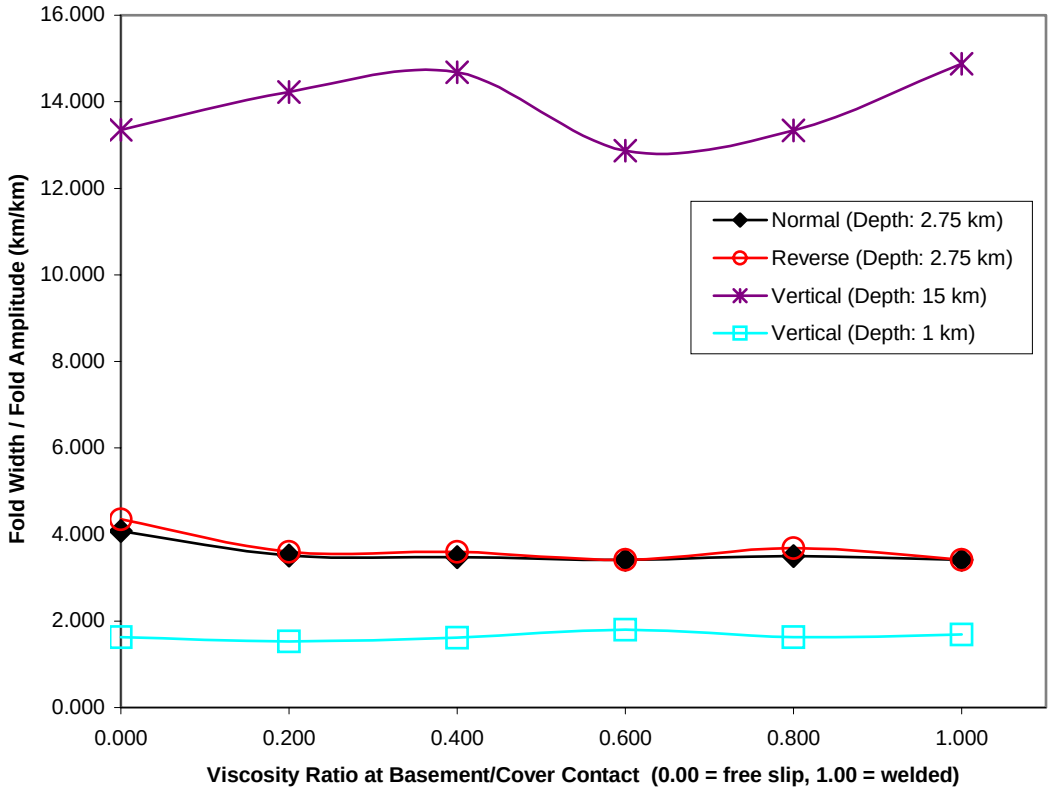

Figure 22. It appears that the effect of the contact behavior is variable at larger depths (15 km), but there are large errors associated with these measurements. However, the effect at small depths (1 km) is indeterminable. Therefore, at small depths, the behavior of the contact is least significant.

The results in the above paragraphs pertain to general statements about displaced buried faults; however, they can be employed to investigate the geometry of observed folds. The application of the model results must be warranted, however. In the case of the trap-door structure, observations of other kink-folds and faults justify the study. In the *Discussion* section, model results prescribe a mechanical explanation for the geometry of the trap-door structure.

6. Discussion

The presence of two *en echelon* monoclines in the study area suggests two buried *en echelon* features. The features may be buried faults or igneous intrusions, but given the consistency between the orientation and geometry of the trap-door structure and other kink-like folds (Cummings et al., 2000; Hess, 1998) in the Oregon-Idaho graben, buried *faults* are the most likely explanation. The fault geometry that best fits all the geologic evidence is a pair of N30E striking, shallow (0.24-0.77 km deep), high-angle (75-90°), right-stepping, *en echelon* faults. The distance between the faults at the step-over is equal to the width of the trap-door structure. The step-over should occur at the mid-region of the trap-door structure. This understanding of the subsurface structure has implications for how NE features within the Dry Creek Buttes fault zone evolved, and perhaps, also for other NE features in the Oregon-Idaho graben. This relationship may be extended speculatively to the trans-Challis fault zone described by Kiilsgaard and Fisher (1995). The trans-Challis fault zone is approximately N25E to N35E striking, and has similar structural and stratigraphic histories to the Oregon-Idaho graben. The goal in following paragraphs is to identify the correct fault type and then use the model to infer layer rheology.

6.1 Solutions for the Trap-door structure

The trap-door structure is a narrow band of deformation like that at the tip of a fault. There are no indications in the study area that there is a strong regional-dip that

would result from rotation during movement on a curved fault surface. Therefore, a listric fault could only have formed the surface folds if the rotated the rotated blocks were long. The Dry Creek Buttes fault zone is 2-3 km wide and contains three folds—the two trap-door opposite facing monoclines and the kinks in the Burnt Mountain strand. As Figure 19 indicates, the space between buried faults in the Dry Creek Buttes fault zone would need to be much greater than 3 km to produce folds without significant rotation. Therefore, straight faults best explain the faulting.

The model "experiments" allow for fault dips that vary from 45° to 90° (Figure 18). Field mapping of the faults in the Oregon-Idaho graben can be used to put further restrictions on fault angles. Regionally, fault angles tend to be very high, 75° to 90°. Thus the faults responsible for the trap-door structure folds are likely to lie within this range. In the following analysis, a fault angle of 83° is assumed.

Vertical changes in the material properties of the folded layers (anisotropy) also effects fold geometry (Figure 23). The degree of anisotropy between buried layers is unknown, but may be estimated using the model. To do this, the viscosities of stiff (1) and soft (2) layers are partitioned into their shear, μ_s, and normal, μ_n, components (Johnson and Fletcher, 1994):

$$\frac{\mu_2}{\mu_1} = \frac{\left(1 + \frac{t_2}{t_1}\right)\left(\frac{\mu_2}{\mu_1}\right)}{\frac{t_2}{t_1} + \frac{\mu_2}{\mu_1}} \qquad (1.\ 11)$$

$$\frac{\mu_n}{\mu_1} = \left(\frac{1}{\left(1 + t_2 / t_1\right)} \right) \left(1 + \frac{\left(t_2 / t_1\right)}{\left(\mu_2 / \mu_1\right)} \right), \ \mu_2 \langle \mu_1 \qquad (1.\ 12)$$

The components of viscosity are normalized to the viscosity of the stiff layers and *t* represents layer thickness. For the trap-door structure, the expressions estimate a range of anisotropy from 1.00 (isotropic) to 5.00 (highly anisotropic). Figure 24 shows two regression lines from experiments for deformation above a reverse fault with a dip of 83°. The two lines are boundaries for the range of possible fold geometries generated by variations in layer properties.

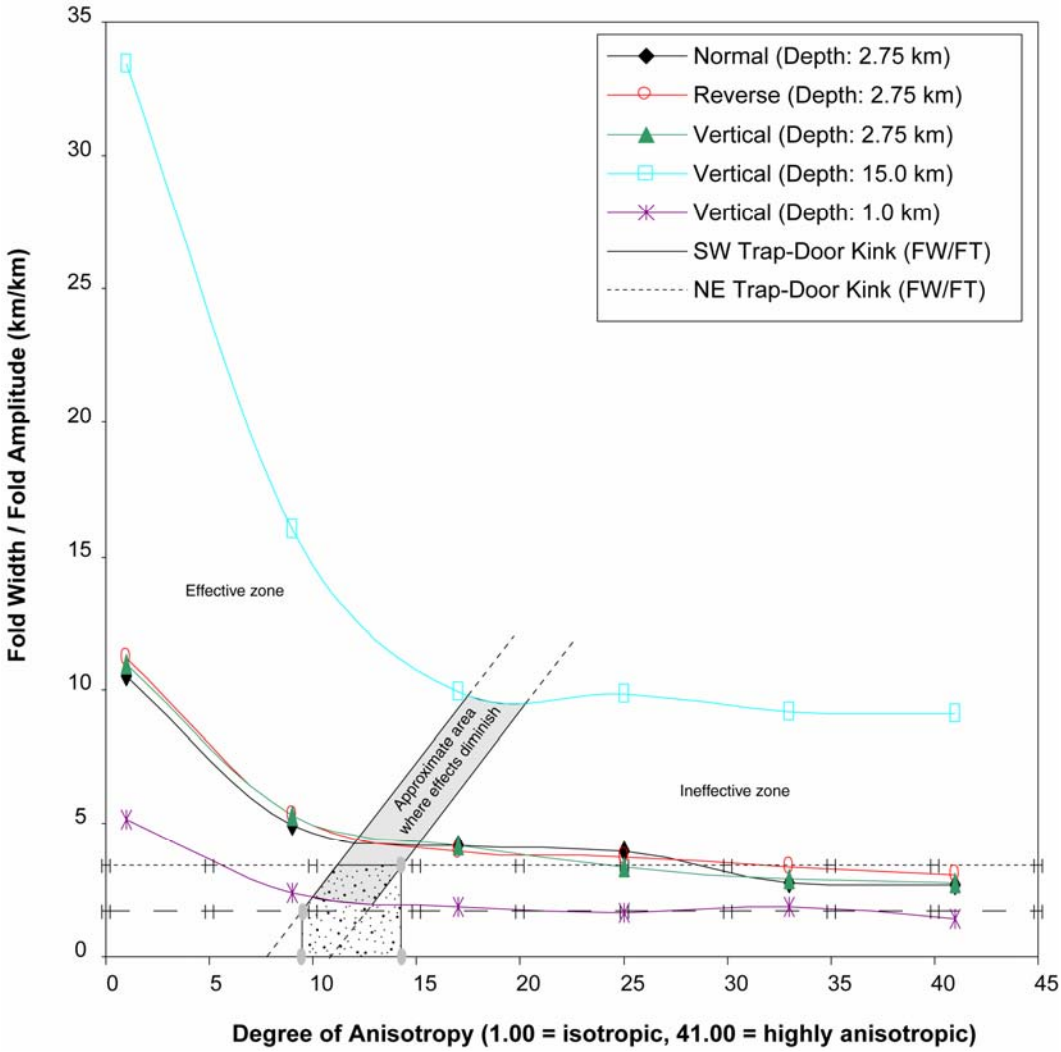

Figure 23. The approximate area where anisotropic effects diminish on the trap-door structure (stippled) is estimated from the mapped fold width to amplitude ratio and Figure 20. The estimated anisotropy range for the layers of the trap-door structure is from 1.00 to 5.00. The anisotropy range for the trap-door structure is clearly within the effective zone, thus anisotropy has a role in deformation geometry.

For the trap-door structure, fold amplitude and fold width were measured from down-plunge views neglecting the fault displacements along the kink-hinges (Figure 25). According to these measurements, the northeast section has a fold width of 0.765 km, and fold amplitude of 0.225 km. The southwest section has a fold width equal to 0.565 km, and amplitude equal to 0.320 km. The model predicts fault depth ranges of

0.38 km to 0.45 km in the northeast section, and 0.24 to 0.45 km in the southwest section. These estimates are made using the average thickness of Tss_4, Tss_5, and Tss_6. In reality, the thickness of the stiff layers varies from 0.40 km to 0.100 km, but the range of anisotropy accommodates this variability. Tuning the anisotropy would allow me to force the faults to be at exactly the same depth, but doing so would not yield meaningful insight into the problem.

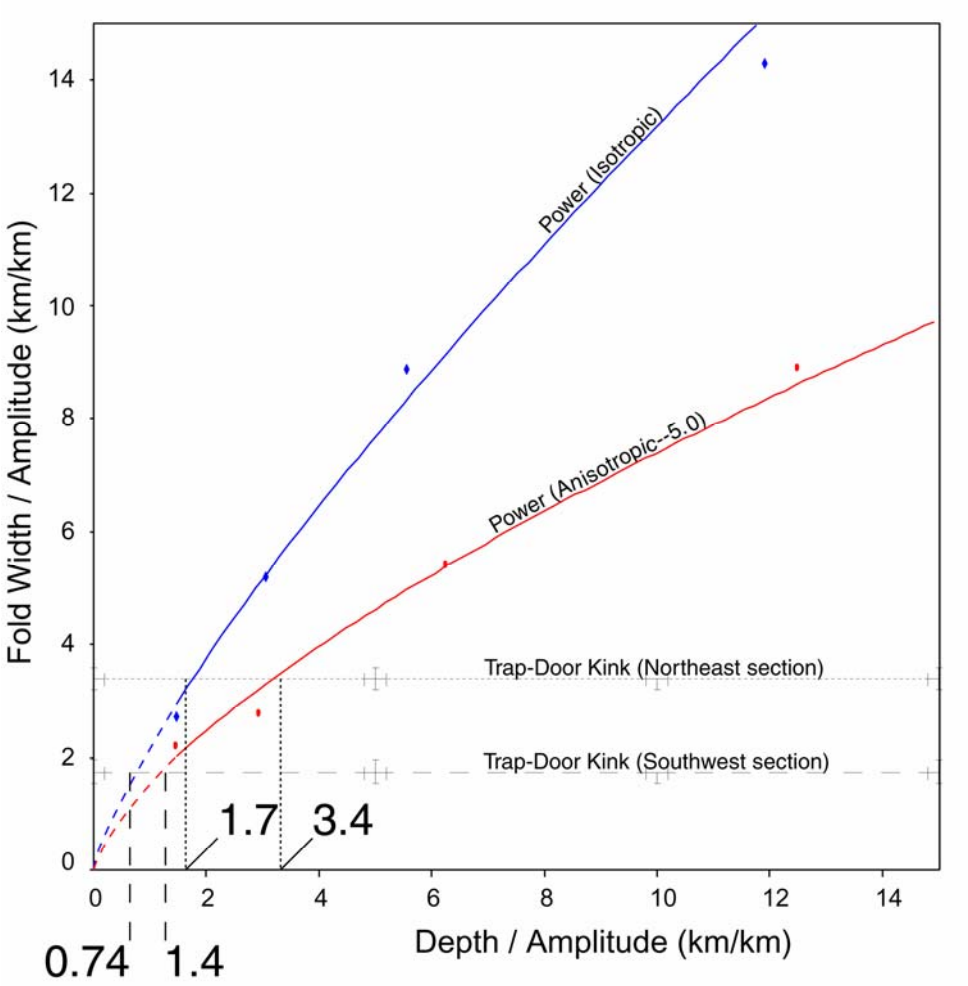

Figure 24. This chart shows the range of possible fold geometries above high-angle (83°) buried faults. The estimated throw is equal to the fold amplitude. Mapped width to amplitude ratios for the two folds are plotted and used to identify the range of fault depths implied by the model.

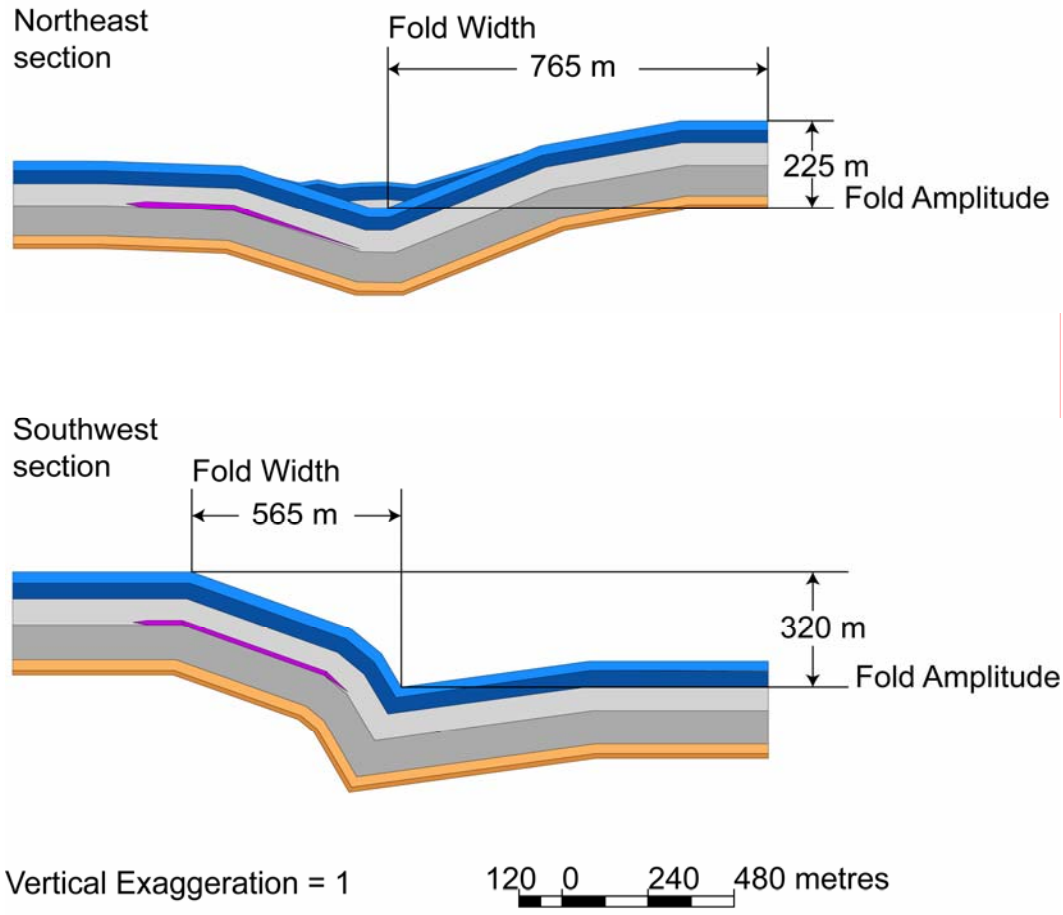

Figure 25. This diagram shows how the fold geometry was measured.

Locations of the buried faults and estimated amounts of throw are mapped in Figure 26. The dashed faults represent the interpreted location of each fault, and the values of throw are approximated from the geometry of the fold prior to kink-hinge faulting. The faults may continue along strike beyond the map area.

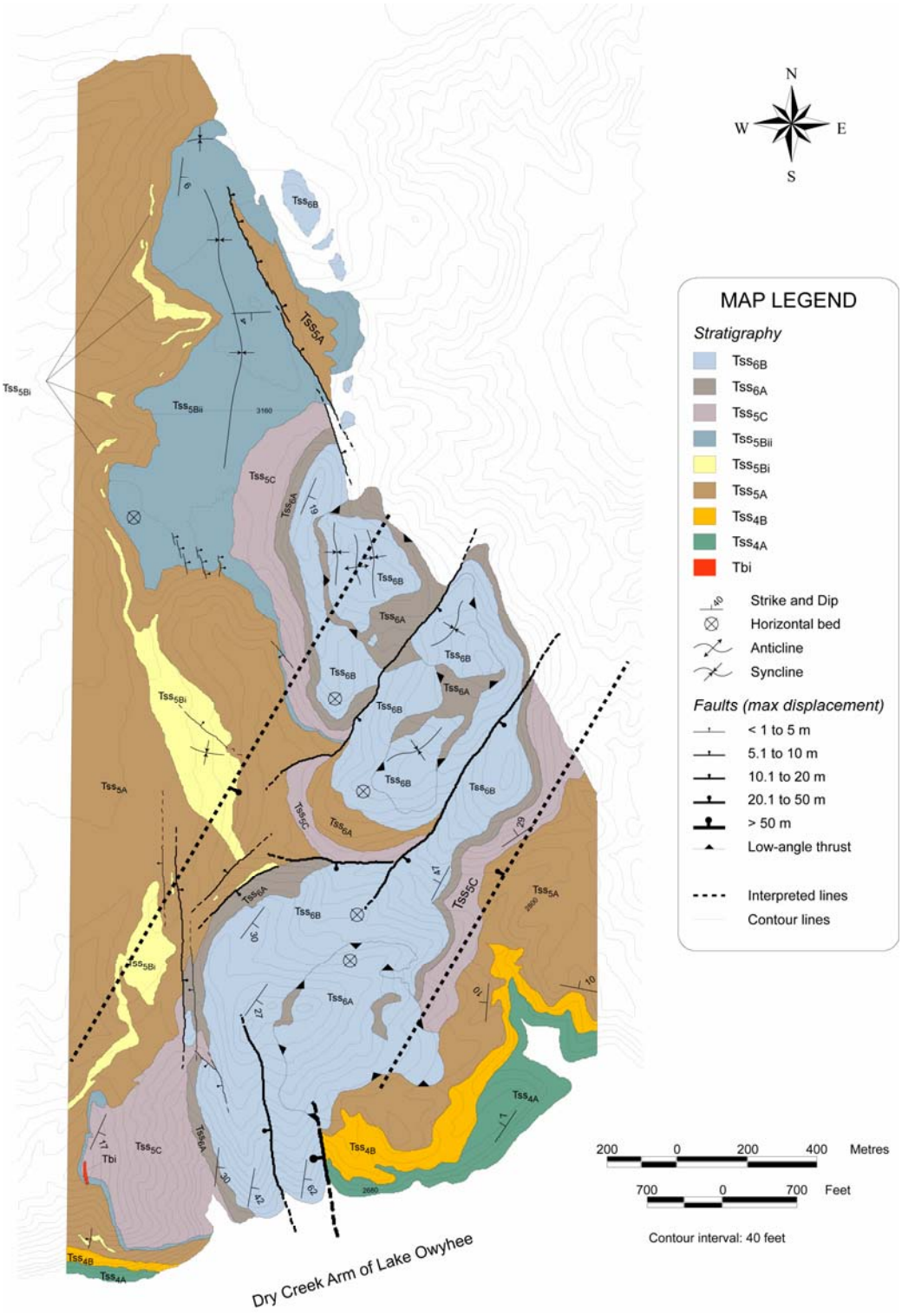

Figure 26. Summary map showing the interpreted locations and trends (largest dashed lines) of buried faults. The faults may extend beyond the map area.

6.2 Implications

Subtle NE-striking kink-like folds exist within the graben but are too small to be seen on smaller scale maps. For example, on the 30 x 60 minute geologic map by Ferns et al., (1993), the trap-door structure is expressed as four north-striking faults, four NW striking faults, and two or three NE striking faults (Figure 27). The folding within the Burnt Mountain strand is also expressed as faulting (Figure 27). As a result, these features, and others like them, are overlooked in interpretations of the regional structural evolution. Perhaps a symbol could represent such features on a map.

Perhaps some speculation will bring light to the problem. The NE-striking trans-Challis fault zone described by (Kiilsgaard and Fisher, 1995) has evolved in a similar structural and stratigraphic fashion as the Oregon-Idaho graben. The relative timing between the trans-Challis fault zone and the Oregon-Idaho graben is indistinguishable. Furthermore, the trans-Challis fault zone is situated in Idaho such that it is oriented in the direction of the Oregon-Idaho graben. An interpretation is that the subtle NE-striking folds and buried faults of the Oregon-Idaho graben are a buried extension of the trans-Challis fault zone. However, the trans-Challis fault zone is untraceable across the 10.5 Ma western Snake River Plain. The western Snake River Plain, on the other hand, developed after the major displacements within the trans-Challis fault zone (Kiilsgaard and Fisher, 1995) and Oregon-Idaho graben (Cummings

et al., 2000), thus the evolution of the western Snake River Plain may have destroyed any record of the trans-Challis fault zone in the area.

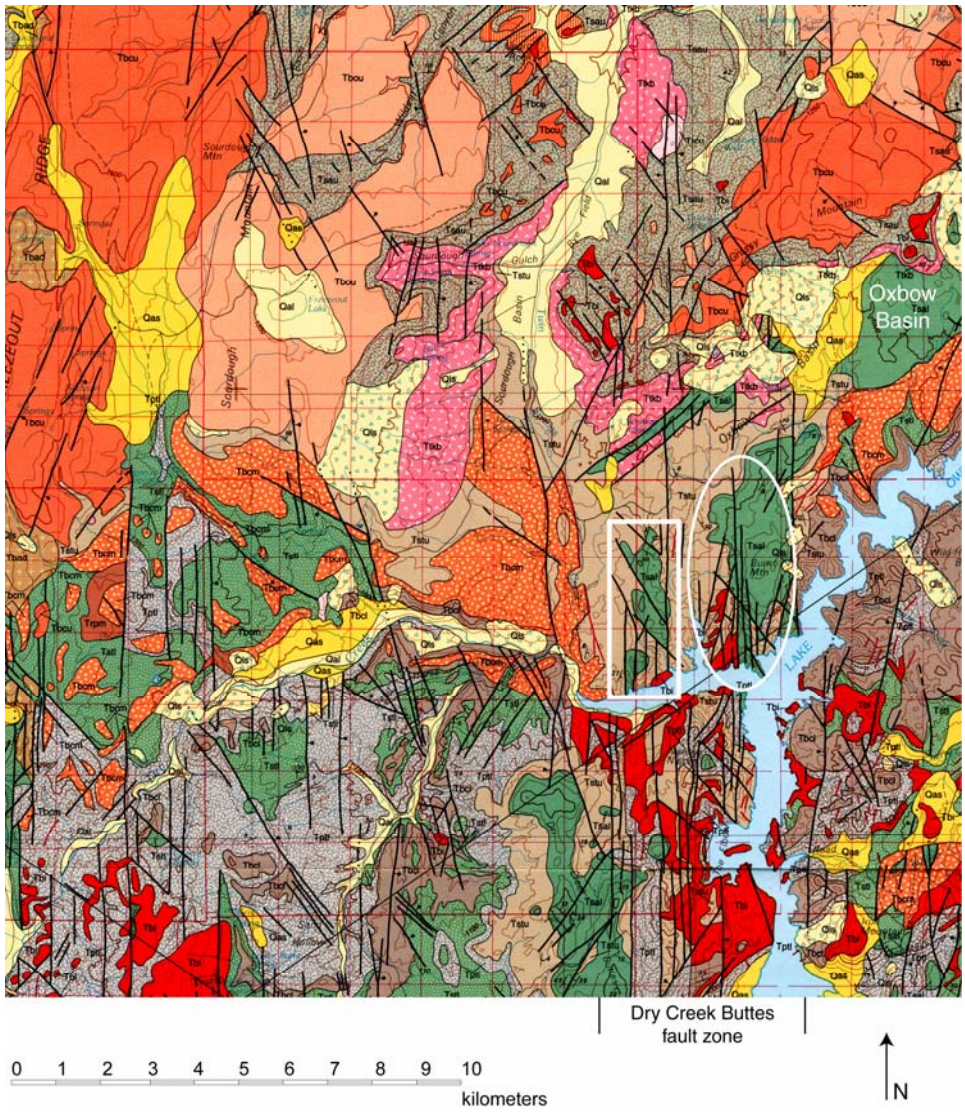

Figure 27. Portion of the 30 x 60 minute geologic map around Lake Owyhee (Ferns et al., 1993). The trap-door structure (white rectangle) and the Burnt Mountain strand (white ellipse) are expressed as sets of faults rather than faulted folds.

7. Conclusions

The evolution of the trap-door structure began with a rotation of the local stress field from NE to NW, as recorded in joint patterns. Early on, layer parallel slip resulted in repeated units, followed by the formation of two monoclinal folds. The monoclinal folds developed as a set of smaller kink-folds across the fold limbs. The timing between formation of the joints and deformation bands could not be determined. However, it is knowing that the deformation bands formed prior to, parallel to, and near the faults that leads me to think each kink-hinge along the monoclinal fold served as premonitory shear zones for the exposed faults, thus, releasing strain during folding. I also believe that the monoclines acted as premonitory shear zones to the propagating buried structure.

One of two structures is possible; therefore, one of two processes is responsible for the current mapped geometry of the trap-door structure: igneous intrusions or buried faults. The geometry is similar to that above margins of intrusions, and the presence of dikes and sills in the study area support such a conclusion. Unfortunately, the bottom contact of the sills is unexposed, so I was unable to determine if they are folded. The trap-door structure geometry is also similar to geometries expected above displacing buried faults. The structural evolution of the Oregon-Idaho graben indicates faults. The presence and consistent orientation of kink-like folds throughout the Oregon-Idaho graben indicates faults, and certainly, the Dry Creek Buttes fault

zone indicates deformation around faults. Therefore, buried faults are the more likely explanation.

Modeling and the mapped geometry indicate that a pair of NE-striking, high-angle *en echelon* faults are buried beneath the trap-door structure. The fault-blocks are 0.24 km to 0.77 km deep, and have displacements ranging from 0.225 km to 0.320 km.

The geometry of the trap-door structure appears on published maps as faults without dip changes across the faults. Other subtle folds rarely turn up on published geologic maps, but the implications for the subtle NE-striking kink-like folds are overlooked in the interpretation of the Oregon-Idaho graben structural evolution.

References

Antonellini, M.A., Aydin, A., and Pollard, D.D., 1994, Microstructure of deformation bands in porous sandstones at Arches National Park, Utah: Journal of Structural Geology, v. 16, no. 7, p. 941-959.

Aydin, A., and Johnson, A.M., 1978, Development of faults as zones of deformation bands and as slip surfaces in sandstone: Pure & Applied Geophysics, v. 116, p. 931-942.

Aydin, A., and Johnson, A.M., 1983, Analysis of faulting in porous sandstones: Journal of Structural Geology, v. 5, no. 1, p. 19-31.

Camp, V.E., Ross, M.E., and Hanson, W., 2000, Volcanic stratigraphy of the middle and south forks of the Malheur River gorge, eastern Oregon: Geological Society of America, Cordilleran Section, 96th annual meeting: Abstracts with Programs - Geological Society of America, v. 32, no. 6, p. 7.

Cruikshank, K.M., and Aydin, A., 1995, Unweaving the joints in Entrada Sandstone, Arches National Park, Utah, U.S.A.: Journal of Structural Geology, v. 17, no. 3, p. 409-421.

Cummings, M.L., 1991a, Geology of the Deer Butte Formation, Malheur County, Oregon; faulting, sedimentation and volcanism in a post-caldera setting: Sedimentary Geology, v. 74, no. 14, p. 345-362.

Cummings, M.L., 1991b, Relations among volcaniclastic sedimentation, volcanism, faulting, and hydrothermal activity west of Lake Owyhee, Malheur County, Oregon, *in* Geology and ore deposits of the Great Basin: Geological Society of Nevada Symposium Proceedings, p. 111-132.

Cummings, M.L., Evans, J.G., and Lees, K.R., 2000, Stratigraphic and structural evolution of the middle Miocene synvolcanic Oregon-Idaho Graben: GSA Bulletin, v. 112, no. 5, p. 668-682.

Ekren, E.B., 1982, Cenozoic stratigraphy of western Owyhee County, Idaho, *in* Breckenridge, B. B. a. R. M., ed., Cenozoic Geology of Idaho: Idaho Bureau of Mines and Geology Bulletin: Moscow, Idaho, Idaho Bureau of Mines, p. 215-235.

Evans, J.G., 1990a, Geology and mineral resources map of the Jonesboro Quadrangle, Malheur County, Oregon: Oregon Department of Geology and Mineral Industries Geologic Map Series GMS-66, scale 1:24,000.

Evans, J.G., 1990b, Geology and mineral resources map of the South Mountain Quadrangle, Malheur County, Oregon: Oregon Department of Geology and Mineral Industries Geologic Map Series GMS-67, scale 1:24,000.

Ferns, M.L., Brooks, H.C., Evans, J.G., and Cummings, M.L., 1993, Geologic map of the Vale 30 x 60 minute quadrangle, Malheur County, Oregon, and Owyhee County, Idaho: Oregon Department of Geology and Mineral Industries Geologic Map Series GMS-77, scale 1:24,000.

Ferns, M.L., and Cummings, M.L., 1992, Geology and mineral resources map of The Elbow quadrangle, Malheur County, Oregon: Oregon Department of Geology and Mineral Industries Geologic Map Series GMS-62, scale 1:24,000.

Hamming, R.W., 1973, Numerical methods for scientists and engineers: New York, NY, Dover Publications.

Hess, S.R., 1998, Structural Evolution of the Dry Creek Buttes Fault Zone, Oregon-Idaho Graben, Malheur County, Oregon [MS thesis]: Portland, OR, Portland State University, 130 p.

Johnson, A.M., 1995, Orientations of faults determined by premonitory shear zones: Tectonophysics, v. 247, p. 161-238.

Johnson, A.M., and Fletcher, R.C., 1994, Folding of Viscous Layers: New York, USA, Columbia University Press, 461 p.

Johnson, K.M., and Johnson, A.M., 2002, Mechanical analysis of the geometry of forced folds: Journal of Structural Geology, v. 24, no. 3, p. 401-410.

Kiilsgaard, T.H., and Fisher, F.S., 1995, Trans-Challis fault system terrane, *in* Fisher, F. S., and Johnson, K. M., eds., Geology and mineral resource assessment of the Challis 1 by 2 degree quadrangle, Idaho: Washington, US Geological Survey Professional Paper, p. 50-52.

Kittleman, L.R., Green, A.R., Haddock, G.H., Hagood, A.R., Johnson, A.M., McMurray, J.M., Russell, R.G., and Weeden, D.A., 1967, Geologic map of the Owyhee region, Malheur County, Oregon: University of Oregon Museum of Natural History Bulletin, scale 1:125,000.

Kittleman, L.R., Green, A.R., Johnson, A.M., McMurray, J.M., Russell, R.G., and Weeden, D.A., 1965, Cenozoic stratigraphy of the Owyhee region, southeastern Oregon: University of Oregon Museum of Natural History Bulletin, v. 1, 45 p.

Lanczos, C., 1961, Applied Analysis: Englewood Cliffs, NJ, Prentice Hall.

Lees, K.R., 1990, Magmatic and tectonic changes through time in the Neogene volcanic rocks of the Vale area, Oregon, North Western USA [Ph.D. dissert.]: Milton Keynes, UK, Open University, 284 p.

Lekhnitskii, S.G., 1981, Theory of Elasticity of an Anisotropic Body: Moscow, Russia, Mir Publishers, 430 p.

Orr, E.L., and Orr, W.N., 1999, Geology of Oregon: Dubuque, Iowa, Kendall/Hunt Publishing Company, 254 p.

Patton, T.L., and Fletcher, R.C., 1995, Mathematical block-motion model for deformation of a layer above a buried fault of arbitrary dip and sense of slip: Journal of Structural Geology, v. 17, no. 10, p. 1455-1472.

Patton, T.L., and Fletcher, R.C., 1998, A rheological model for fractured rock: Journal of Structural Geology, v. 20, no. 5, p. 491-502.

Walker, G.W., and Robinsons, P.T., 1990, Paleocene (?), Eocene, and Oligocene (?) rocks of the Blue Mountains Region: U.S. Geological Survey Professional Paper, p. 13-27.

Appendix—Maps

Plate 1—Analytic map of the trap-door structure

Plate 2—Geologic map of the trap-door structure